Hypocenter relocation in Groningen using the double-difference method

AW-Graduation Research, Earth Sciences GEO4-1520

J.J.M. van Weers (4243471)
jaspervanweers@hotmail.com

1st supervisor: Hanneke Paulssen
2nd supervisor: Matthew Herman

Universiteit Utrecht

Faculty of Geosciences
University Utrecht

November 29, 2019

Abstract

Production from the Groningen gas field has resulted in induced seismicity due to reactivation of existing faults in the subsurface ever since 1991. In the same year, the Royal Netherlands Meteorological Institute (KNMI) deployed a pilot borehole with a number of geophones at depth. With time the network has evolved in a dense geophone network in the past 5 years. A denser network allows for higher accuracy in determining hypocenter locations. These locations are especially important because they indicate which faults in the subsurface are seismically active and thus can result in an improved seismic hazard analysis. In the hypocenter method that is used by the KNMI to determine hypocenter locations, the focal depth is fixed to 3 km as this is the average gas reservoir depth. In this research, we explore the viability of hypocenter relocation in the Groningen region by means of the double-difference method. This method is based on the similarity of ray paths if the epicentral distance between two events is small relative to the event-station distance, for a common seismic station. With this, travel time differences can be attributed to relative hypocenter distances between those events within the source area, thus minimizing the effects of travel time variations caused by unknown subsurface structures. *HypoDD* from Waldhauser and Ellsworth (2000), a double-difference relocation program based on ray theory with a 1D velocity model, is used for this purpose. We have found that under some constraints, hypocenters can be relocated with an estimated uncertainty of 240 m in both the vertical and horizontal plane. Compared to other methods, the double-difference method has proved to be a viable hypocenter relocation method. Additionally, our results indicate that the gas source rock, gas reservoir, cap rock and a shallower anhydrite layer likely all are seismically active, with faults present in the gas reservoir extending into deeper formations.

1 Introduction

Production from the Groningen gas field has resulted in induced seismicity since 1991 due to the reactivation of existing faults. Most of the earthquakes listed in the Royal Netherlands Meteorological Institute (KNMI) earthquake catalog fall in the local magnitude range of 0.5 to 2.5 (KNMI, 2019a). Due to several expansions of the seismic network by the KNMI in and surrounding the Groningen gas field in the past 30 years, the ability to detect events, especially those with magnitudes smaller than 1.5, has drastically improved (Dost et al., 2017). The KNMI borehole geophone network has evolved from 1 pilot borehole in 1991 to 8 additional boreholes in 1995, 3 more in 2010 and a major rollout of 85 extra since 2014. In these boreholes, geophones have a vertical spacing of 75 m, 50 m, 30 m and 50 m, respectively. This spacing also directly indicates the depth of the uppermost geophone. The deepest geophone is located at 200 m depth for the deployment of 1995 and since 2014 (KNMI, 2019b).

A denser seismic network allows for higher accuracy in locating hypocenters. Better locations can result in a better determination of active subsurface faults and thus can result in an improved seismic hazard analysis. Network geometry, P- and S-wave pick accuracy and knowledge of the subsurface are factors in accurately determining hypocentral parameters. Compared to the accuracy in the horizontal plane, the focal depth resolution is inaccurate (Dost et al., 2017). Determining the focal depth is especially challenging because of the strong trade-off between source depth and origin time (Billings et al., 1994). Further expansion of the seismic network and the use of a more detailed local velocity model did not yield improved approximations for the source depth with the current P-wave *HYPOCENTER* method, by Lienert et al. (1986), used by KNMI (Spetzler and Dost, 2017). Because on average the reservoir rock is located at 3 km depth, the KNMI has set this value as default focal depth for all events.

Several techniques have been developed to more precisely relocate the initially found earthquake hypocenters. Amongst these are the equal differential time (EDT) method (Theunissen et al., 2012), also known as the maximum intersection (MAXI) method (Font et al., 2004), and the double-difference (DD) method (Waldhauser and Ellsworth, 2000). The EDT method is based on the notion that the difference in observed travel times at a station pair is equal to the calculated travel time difference for those stations. A hyperbolic surface can be found with a collection of points satisfying the description. The location with most intersecting EDT surfaces is considered the hypocenter location. The EDT relocation depends on detailed 3D velocity models (Theunissen et al., 2012). The double-difference method is based on ray path similarity from source to receiver for an event pair to multiple receivers. This results in travel time differences that can be attributed to relative hypocenter distances within the source area (Waldhauser and Ellsworth, 2000).

Our main objective is to explore the viability of

hypocenter relocation in Groningen using the double-difference method. Additionally, if it proves to be a viable option, we want to compare the results obtained through the double-difference method with other (re)location methods.
For this double-difference relocation, the program *HypoDD* (version 1.3) is used (Waldhauser, 2001), which minimizes residuals between observed and calculated travel times for an event pair based on a 1D layered velocity model. These calculated travel times are established through ray tracing. The resulting hypocentral parameters are compared to those listed by the KNMI in their event catalog and those found by Spetzler and Dost (2017) with the EDT method.
We provide an overview of the formations in the subsurface in Groningen in section 2, discuss the double-difference theory and *HypoDD* in section 3, describe the data (pre-)processing stage and choices that are made in section 4 and then proceed with further constraints and event relocation in section 5. We compare our results with different (re-)location methods and supply additional notes on the subsurface geology in section 6 and conclude the study in section 7.

2 Geological setting

In this section, we describe the subsurface of the Groningen area specifically along the ZRP01 well. This well is located near Zeerijp (TNO, 2019). Furthermore, we provide additional information about deeper formations.

The deepest group we consider is the Carboniferous Limestone Group (CL) of Dinantian age (331-359 Ma), which is characterized by its carbonate platforms and carbonate-rich deposits (Kombrink, 2008; Van Adrichem Boogaert and Kouwe, 1997). The occurrence, faults within and distribution of the Carboniferous Limestone Group in the Netherlands is relatively unknown. It is also not known which exact formations are located deeper than the CL. The seismic interpretations listed in chapter 3 of Kombrink (2008) allow for an estimation of the depth of the CL in the Groningen area. Combined with a suitable velocity model the depth of the top of this formation is estimated at 5.3 km.

Directly on top of the CL, the Limburg Group (DC) can be found. It consists of deposits corresponding to a regressive deltaic foreland-basin (Van Wijhe, 1981) of Silesian age (299-331 Ma). This regressive behaviour is interpreted to be caused by regional uplift resulting from the Variscan Orogeny (De Jager, 2007). The Limburg Group is the source rock of the Groningen gas field.

The DC is unconformably overlain by the Upper Rotliegend Group (RO) of late-Permian age (259-265 Ma) (Menning et al., 1988). It mostly consists of porous red-bed type sandstone and acts as the reservoir rock. Faults in the subsurface of Groningen are present in the Rotliegend Group with mainly a NNW-SSE and an ENE-WSW orientation and to a lesser extent with an E-W trend (Figure 1). The majority of these faults were formed in a tectonic rifting phase during the Mid to Late Kimmerian (125-185 Ma) (de Jager and Visser, 2017) as a result of a transtensional faulting of reactivated older faults (De Jager, 2007). Gas production has resulted in the present-day reactivation of these faults (Spetzler and Dost, 2017). The vertical extent of these faults to older formations is unknown.

The Rotliegend is overlain by the Zechstein Group (ZE), also of late-Permian age (252-259 Ma). The Zechstein is largely composed of evaporites such as rock salts and anhydrites. The latter is characterized by high seismic velocities, low permeability and high stiffness, whereas the rock salts are soft and ductile and show halokinetic deformations (de Jager and Visser, 2017). In the sonic log of well ZRP3, two anhydrite layers can be identified (Figure 2). These are

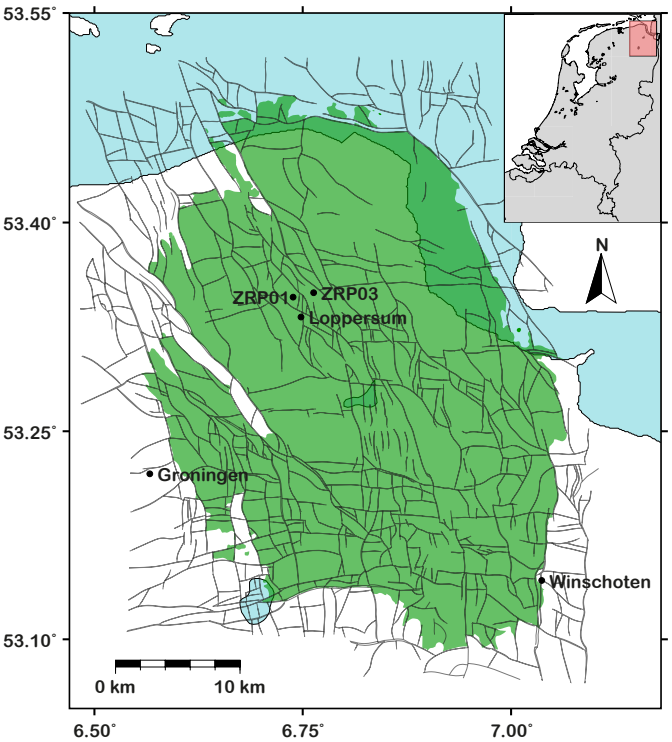

Figure 1: Extent of the Groningen gas field and faults at the top of the Rotliegend formation (depth locally ranges between 2.5 and 3.2 km). The location of Loppersum and the ZRP03 well log are indicated. The estimated original amount of gas is 2700 billion cubic meters (bcm) (NAM, 2011). Gas field and fault data are by courtesy of the Nederlandse Aardolie Maatschappij (NAM).

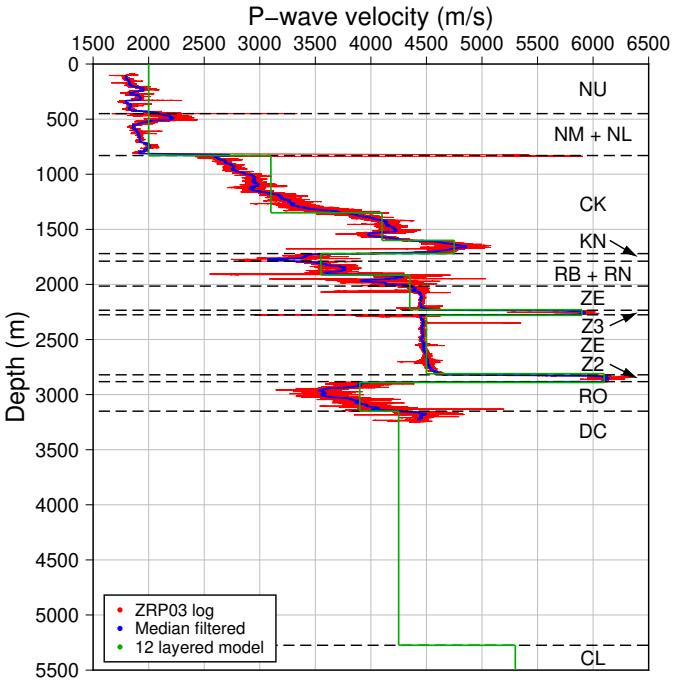

Figure 2: Seismic velocity with depth at well ZRP3 in red. Geological layer interpretations are given with the dashed lines. The average of approximately every 6 m, obtained with a moving window filter, is given in blue and a 12 layered velocity model with uniform velocity for each layer in green. The latter is discussed in section 5 in more detail. The velocities of these layers are manually selected. Well data is by courtesy of the NAM.

the Z2 and Z3 from bottom to top, respectively (Van Gent et al., 2011). The lowermost anhydrite layer is located directly above the Upper Rotliegend and serves as the cap rock of the gas field (Romijn, 2017). Due to the ductile nature of the rock salt portion of the Zechstein, faults in the Rotliegend do not extend into the Zechstein (de Jager and Visser, 2017).

On top of the Zechstein are the Upper and Lower Germanic Trias groups, RN and RB, respectively. These groups are distinguished by clastic materials in shallow marine or fluvial setting of Triassic age ($\sim$ 200-252 Ma). Due to salt tectonics during the Kimmerian rifting phase, perforations by salt domes in the Triassic aged deposits can be observed primarily in the northern part of the Netherlands (Geluk, 2007).

The RN and RB deposits are unconformably overlain by the relatively thin Rijnland Group (KN), characterized by silt or clay-sized clastic sedimentary rocks (Van Adrichem Boogaert and Kouwe, 1997) of early Cretaceous age (100-$\sim$ 145 Ma).

The Chalk Group (CK), consisting of mainly limestones deposited in a shallow marine environment, overlies the Rijnland Group (Van Adrichem Boogaert and Kouwe, 1997). This formation is of late Cretaceous age (66-100 Ma)

On top of the Chalk Group is the North Sea Group (NSG), which is deposited from 66 Ma up to the present day. The North Sea Group is subdivided in the Lower, Middle and Upper North Sea Group (NL, NM and NU, respectively). Every single interface in the North Sea Group is unconformable. Both the NL and the NM are predominantly marine deposits whereas the NU is deposited in a shallow marine setting (Van Adrichem Boogaert and Kouwe, 1997).

3 *HypoDD*

The *HypoDD* program by Waldhauser (2001) is a double-difference method based on the assumption that if the epicentral distance between two events, with a common seismic station, is small relative to the event-station distance, the ray paths from these events to the station are similar for the majority of the ray path. Thus, the travel time difference can be mapped exclusively to relative hypocenter distances between the events in the source area (Waldhauser and Ellsworth, 2000). This is depicted in a schematic manner in Figure 3. Because the travel time differences can be attributed to relative hypocenter shifts in the source region, location errors resulting from unknown or poorly constrained subsurface velocity structure can be minimized (Waldhauser et al., 1999).

The description of *HypoDD* below is subdivided in three subsections: the double-difference theory, the catalog data pre-processing script *ph2dt* and *HypoDD*. For the corresponding input and output file formats the reader is referred to Waldhauser (2001).

3.1 Double-difference theory

The arrival time of a seismic ray for event i to station k along the ray path is defined as

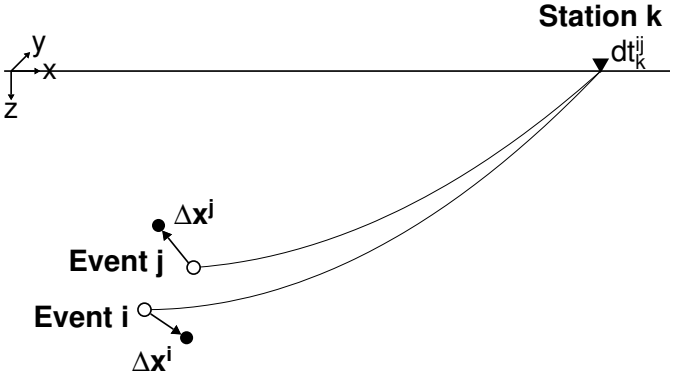

Figure 3: Schematic overview of the double-difference method, with similar ray paths away from the source area. As such, travel time differences measured at the station contribute to hypocenter relocation by $\Delta \mathbf{x}$ close to the sources.

$$T_k^i = \tau^i + \int_i^k u ds, \tag{1}$$

where τ denotes the origin time, u the slowness field and ds a ray path element. Equation 1 is non-linear and can be linearized by a truncated Taylor series expansion (Geiger, 1910). The linear dependence between the travel time residual r and variations of the hypocentral parameters, i.e., location and origin time, $\Delta\mathbf{m}^i = (\Delta x^i, \Delta y^i, \Delta z^i, \Delta\tau^i)$, can be described as

$$\frac{\partial t_k^i}{\partial \mathbf{m}} \Delta\mathbf{m}^i = r_k^i. \tag{2}$$

The residual r_k^i is defined as the difference between the observed travel time and the calculated travel time for event i and station k.

The relative hypocentral parameters for an event pair i and j is given by the difference between Equation 2 for those events as

$$\frac{\partial t_k^i}{\partial \mathbf{m}} \Delta\mathbf{m}^i - \frac{\partial t_k^j}{\partial \mathbf{m}} \Delta\mathbf{m}^j = dr_k^{ij}, \tag{3}$$

with dr_k^{ij} the differential travel time residual,

$$dr_k^{ij} = (t_k^i - t_k^j)^{obs} - (t_k^i - t_k^j)^{cal}, \tag{4}$$

between the two events. This is also referred to as the double-difference.

Relocating events with respect to each other requires finding the changes in location (Δx,Δy,Δz) and origin time ($\Delta\tau$) for each event pair. A system of linear equations can be formed by combining Equation 3 for all event pairs for all stations to

$$\mathbf{WGm} = \mathbf{Wd}. \tag{5}$$

In this equation, $\mathbf{W}$ denotes a diagonal weighting matrix of size $M \times M$ with M the number of double-difference observations, $\mathbf{G}$ the sparse $M \times 4N$ matrix of partial derivatives with N the number of events, $\mathbf{m}$ a vector of length $4N$ containing the changes in hypocentral parameters that are to be found and $\mathbf{d}$ the double-difference data vector of length M. Poor linkage between events can result in an ill-conditioned $\mathbf{G}$ and thus numerical instability. To prevent this a damping factor λ can be applied, rewriting Equation 5 to

$$\mathbf{W}\begin{bmatrix}\mathbf{G}\\ \lambda\mathbf{I}\end{bmatrix}\mathbf{m} - \mathbf{W}\begin{bmatrix}\mathbf{d}\\ \mathbf{0}\end{bmatrix} = 0. \tag{6}$$

In *HypoDD*, the solution can be obtained in two ways, using singular value decomposition (SVD) or using the *LSQR* algorithm of Paige and Saunders (1982) that solves for linear least squares problems by minimizing the residual norm using a conjugate-gradient type method. Equation 5 can be solved using SVD for small datasets and if $\mathbf{G}$ is well-conditioned. *LSQR* is used for larger datasets and ill-conditioned systems by solving for $\mathbf{m}$ in

$$\left\| \mathbf{W}\begin{bmatrix}\mathbf{G}\\ \lambda\mathbf{I}\end{bmatrix}\mathbf{m} - \mathbf{W}\begin{bmatrix}\mathbf{d}\\ \mathbf{0}\end{bmatrix} \right\|_2 = 0. \tag{7}$$

For each iteration, the resulting hypocenter location is tested by reweighting the data quality weights based on both the data misfit compared to either the initial solution for the first iteration or the results of the previous iterative step for further iterations and the inter-event distances. Data with large residuals are either downweighted or rejected for further iterations by a biweight function (Mosteller and Tukey, 1977),

$$W_i = max^3\left(0, 1 - \left(\frac{dr_i}{\alpha \cdot \frac{\mathbf{dr}_{MAD}}{\sigma_{MAD}}}\right)^3\right), \tag{8}$$

with W_i the weighting and dr_i the double-difference of ith equation, α the user set residual threshold, $\mathbf{dr}_{MAD}$ the deviation of the residuals from its median and σ_{MAD} the median absolute deviation (MAD), i.e., for a Gaussian distribution $\sigma_{MAD} = 0.67449$. For inter-event distances the biweight reweighting scheme is

$$W_i = max^3\left(0, 1 - \left(\frac{s_i}{c}\right)^3\right), \tag{9}$$

where s is defined as the distance between two events and c as the user set distance threshold.

3.2 Establishing linkage through *ph2dt*

Data obtained from earthquake catalogs contains, amongst others, absolute first arrival times and estimated origin times. Absolute travel times, derived from the origin times and arrival times, are used as input for *ph2dt*. As *HypoDD* requires travel time differences between pairs of events at the same receiver, the corresponding pre-processing is performed by *ph2dt*.

A network of links between events is established based on the nearest neighbor approach up to a maximum number of neighbors and a maximum search range defined by the user. With this approach, *ph2dt* tries to establish a connection for each event to other events with increasing inter-event distances. Furthermore, for all these event pairs, station observations are selected with an increasing recorder distance, up to a maximum number of observations per pair. A list with parameter abbreviations and their meaning for *ph2dt* can be found in Table A.1. Waldhauser

(2001) recommends being conservative on the selection of data by *ph2dt* and being more rigorous with *HypoDD* input parameters.

3.3 Relocating events through *HypoDD*

Both travel time differences obtained from catalog data (P- and S-picks) and differential travel times obtained through cross-correlation can be used for *HypoDD*. *HypoDD* relocates events with respect to each other by minimizing the residual between calculated and observed travel time differences for event pairs and reiterating with adjusted weights as described in subsection 3.1. A list with parameter abbreviations and their meaning for *HypoDD* can be found in Table A.2. Based on connectivity of events, *HypoDD* divides the events in clusters (if more than one cluster can be found). For each cluster, events are relocated with the set input parameters. Weak linkage between events, outliers and large weighting ranges can cause instability. This results in the need for a very high value for the damping parameter or in a high condition number. Waldhauser (2001) has found, by empirically testing the ideal ranges, that the damping parameter should be in the range of $1 - 100$ and the condition number in the range of $40 - 80$. To negate numerical instabilities, the minimum number of links per event pair can be increased or the reweighting parameters can be changed. After each iteration, the root mean square (RMS) residual, listed in ms, for the system should drop. This generally indicates better suitable hypocenter locations with the specific input parameters.

4 Dataset

Both data obtained through cross-correlation and from catalogs can be used to determine differential travel times with *HypoDD*. In this research, we focus on using the Groningen catalog data from the KNMI.

An overview of the spatial distribution of the geophone network in and surrounding the Groningen area based on the deployment phase is given in Figure 4. Furthermore, the shading indicates whether or not the geophone is used during this research.

The FDSN event web service of the KNMI is used to obtain catalog data for seismic events based on search queries that can be defined by for example start- and end date, magnitude ranges and coordinate ranges (KNMI, 2019a). The data for each event is stored in a QuakeML format file, including picks of P-wave and S-wave arrivals, origin time (UTC), location and depth, magnitude, the RMS of travel time residuals for the arrivals and epicentral distance of stations. The KNMI has ceased using S-wave picks throughout the past decade as difficulties in reliably picking S-waves yielded less accurate hypocenter locations (Spetzler and Dost, 2017). Consequently, we will only focus on P-wave picks.

During the data pre-processing stage, we have removed event and first arrival data for which entries are missing. Travel times are calculated based on the listed origin and arrival times by the KNMI. It should be noted that the origin time is dependent on the hypocentre method and influenced by the chosen velocity model. We have also removed arrivals with negative travel time and arrivals with zero epicentral distance. The latter is chosen because its compatibility with *HypoDD* is unknown.

The deepest geophone on the borehole geophone strings often has the best signal to noise (S/N) ratio. The majority of the first arrivals, 80-89%, depending on the query parameters, are measured at geophones at the deepest geophone string level, which is approximately 200m depth. Consequently, to be consistent, we have chosen to only include arrivals for geophones at approximately 200m depth. Additionally, stations ZLV4 and ZL24 are located at the same well. The latter is removed from the dataset because it has fewer arrivals and as its unclear what effect multiple stations at the same location have on our results.

We define the Groningen region as longitude range 6.48-7.1° (41.42 km) and latitude range 53.07-53.52°

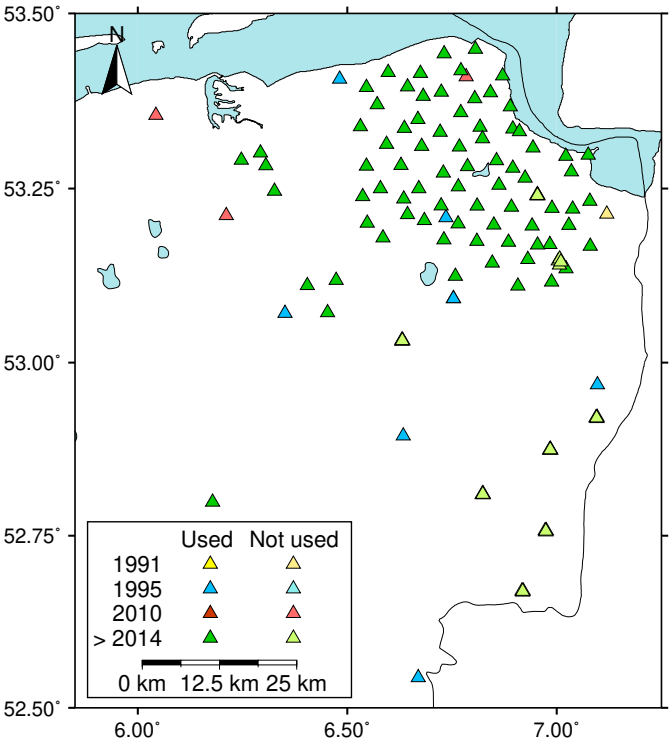

Figure 4: An overview of the phased expansion of the KNMI geophone network. Dark coloured stations have geophones at 200m depth.

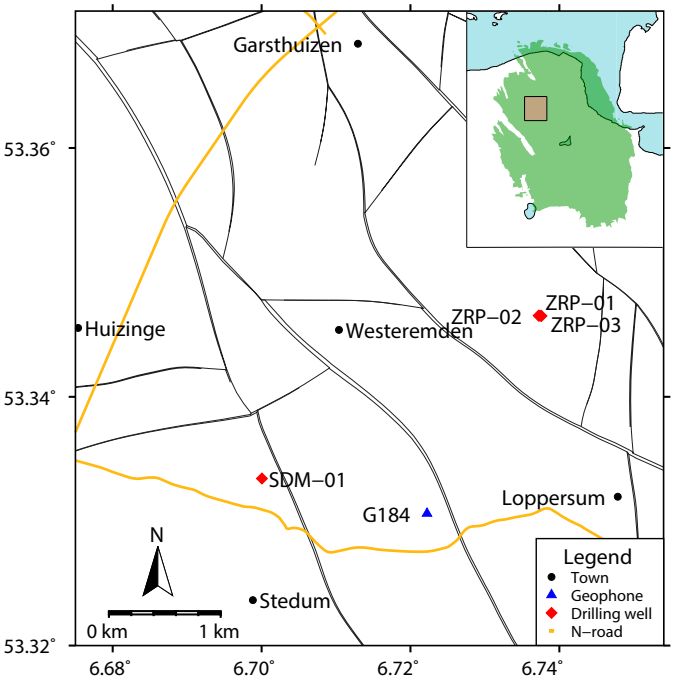

Figure 5: A detailed view of the Loppersum trial area within Groningen. The black lines on the background are the mapped faults at the top of the gas reservoir. Nearby towns, well locations, geophone location and the N-road are added as a reference.

(50.04 km), which includes the entire Groningen gas field, the mapped NAM faults in the Rotliegend and most of the induced seismicity. It should be noted that all coordinates listed in this research are in the world geodetic system (WGS84).

Because it is easier to perform parameter investigation for a smaller region, exploration of *HypoDD* parameters and initial optimization is done for an approximately 5.2 km by 5.6 km area close to Loppersum before moving on to relocating the entirety of the Groningen dataset. This Loppersum region is selected based on the region with large subsidence up to 2013 and high event density in the interactive map of the NAM (NAM, 2019). This trial area has as longitude range 6.675-6.754 and latitude range 53.320-53.371 Figure 5.

We subdivided the data in three different datasets, from 01/01/1995 to 22/10/2014, from 23/10/2014 to 01/04/2019 and from 01/01/1995 to 01/04/2019. We refer to these datasets as pre-2014, post-2014 and full dataset, respectively. Because the data availability is extremely poor prior to 01/01/1995 we have chosen this to be the starting date for the pre-2014 and full dataset. As 23/10/2014 marks the date of the most recent large geophone borehole network expansion by the KNMI in and surrounding Groningen (Figure 4), this date is chosen as the starting date of the post-2014 dataset and the day prior is chosen as the end date of the pre-2014 dataset. We have arbitrarily chosen 01/04/2019 as end date for the post-2014 and full dataset. To ensure that events are large enough to be measured by stations, we set magnitude constraints of 0.85+ and 0.45+ for the pre-2014 and post-2014 datasets date windows, respectively (Dost et al., 2017).

The FDSN query parameters used to download these datasets and the number of events, geophones and measured arrivals within the datasets can be found in Appendix B.

5 Hypocenter relocation

All model runs were executed on an HP EliteDesk 800 G1 tower workstation with an Intel 8 Core i7-4770 processor and a clock speed of 3.40 GHz. Models do not run in parallel, i.e. only a single core is used.

Because Waldhauser (2001) has recommended being conservative with *ph2dt* parameters, i.e., conservative with the data selection, these parameters are not changed during the course of this research. Additional restrictions are imposed on the data through *HypoDD* parameters. The parameter values for *ph2dt* can be found in Table C.1.

5.1 Simplified ZRP3 velocity model

A velocity model containing 11 velocity layers is constructed based on the ZRP3 well data. The velocity of the 11th (bottom) layer, the gas source rock, is set to 4.25 km/s (Akbar, 2018). Because rays do not only travel upwards from the source to the receiver, we want to add a relevant 12th velocity layer for rays that travel directly downwards from the source. As a velocity of approximately 5.1 km/s was found in the layer below the gas source rock (Jagt et al., 2017), an additional 12th velocity layer corresponding to this Carboniferous Limestone Group (CL) is added. The depth of the top of the CL layer is obtained from seismic reflection data (Kombrink, 2008) and the previously found velocities. We estimate the top of the CL to be at approximately 5.3 km depth. The resulting $1D$ 12 layered velocity model is shown in Table C.2 and Figure 2.

5.2 Relocation with 12 layered model

Very small variations in the velocity model in *HypoDD* for the pre-2014 dataset in the Loppersum area has resulted in large differences in hypocentral parameters. Up to the 2014 geophone network expansion, the number of stations was limited to 8 geophones with an azimuthal gap of approximately 130°

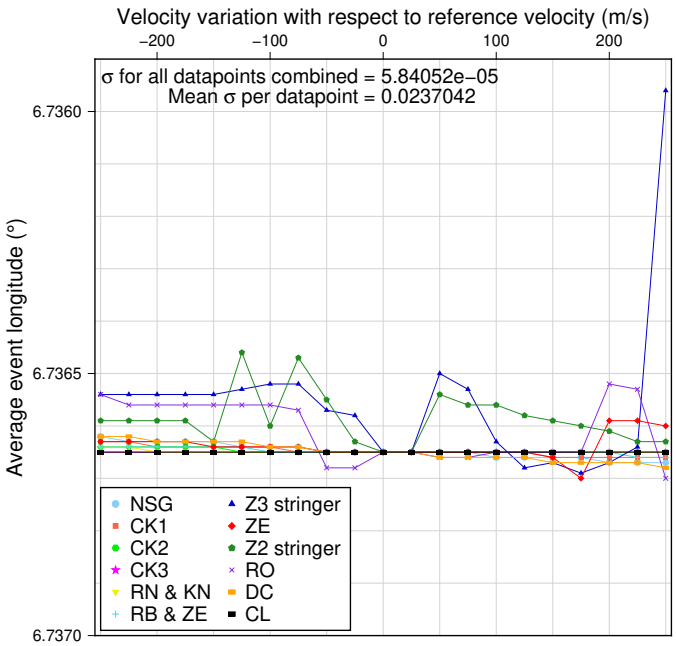

Figure 6: The longitude of the cluster centroid for velocity variations in each layer with respect to the reference velocity (Table C.2). The mean standard deviation per datapoint denotes the average σ on each *HypoDD* run and the σ for all datapoints combined is the standard deviation on the longitude of the centroid for all runs combined. These standard deviations are in degrees. A variation of 0.0001° equals approximately 6.6 m.

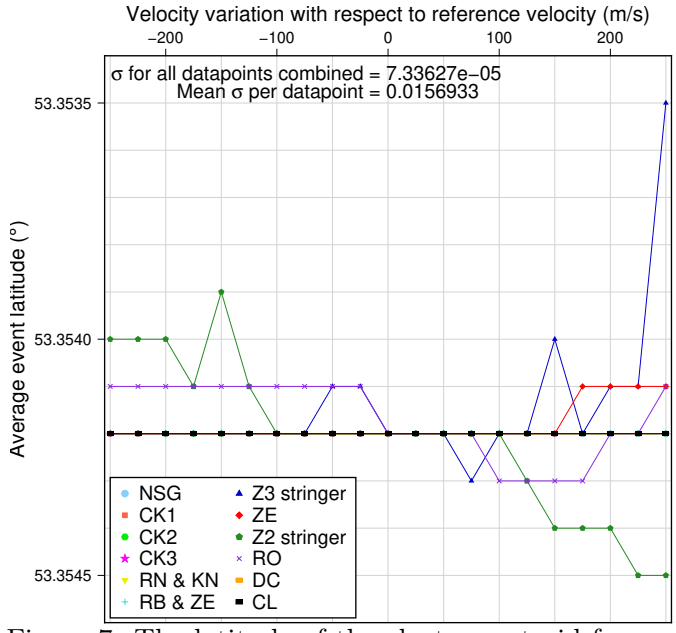

Figure 7: The latitude of the cluster centroid for velocity variations in each layer with respect to the reference velocity (Table C.2). The mean standard deviation per datapoint denotes the average σ on each *HypoDD* run and the σ for all datapoints combined is the standard deviation on the latitude of the centroid for all runs combined. These standard deviations are in degrees. A variation of 0.0001° equals approximately 11 m.

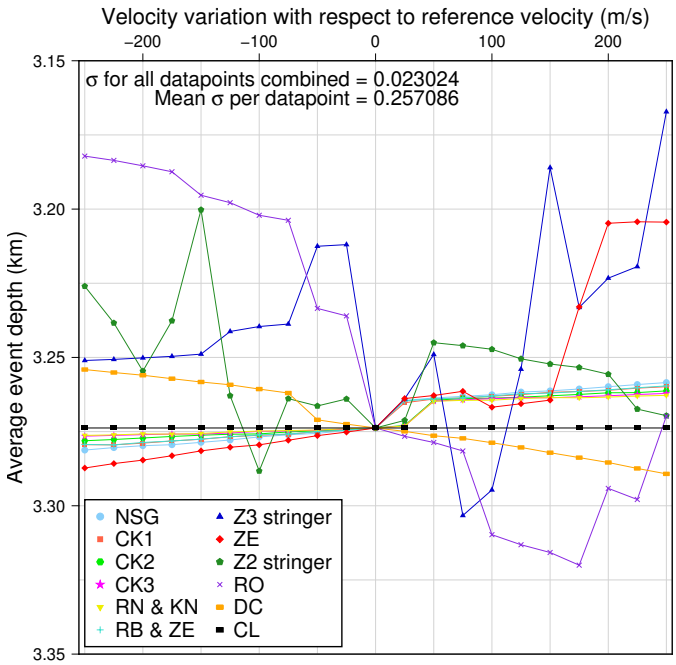

Figure 8: The depth of the cluster centroid for velocity variations in each layer with respect to the reference velocity (Table C.2). The mean standard deviation per datapoint denotes the average σ on each *HypoDD* run and the σ for all datapoints combined is the standard deviation on the depth of the centroid for all runs combined.

(Figure 4). Because these large differences in hypocenter relocation are a result of this sparse network, in combination with poor event connectivity, we refrain from relocating events from prior to 23/10/2014.

By separately varying the *HypoDD* inversion parameters with the 12 layered velocity model in the Loppersum region for the post-2014 dataset, the RMS error is minimized. These input parameters can be found in Table C.3.

In order to determine the effects of variations to the velocity model on the relative relocations, we varied the velocity for each layer separately by increments of 25 m/s. We have performed this for the range of −250 m/s to +250 m/s with respect to the velocity model given by Figure 2. For these variations to the velocity model, the location of the cluster centroid, i.e., the average longitude, latitude and depth, is calculated and compared with respect to the reference location. Tracking the location of the cluster centroid for such variations allows for a better determination of its effects on the dataset. For these variations to the velocity model, the longitude, latitude and depth of the cluster centroid can be observed in Figure 6, Figure 7 and Figure 8, respectively. From the standard deviation for all datapoints combined, we find that the average longitude and latitude of the cluster centroid is relatively stable compared to its

focal depth. Velocity variations within the Z3 and Z2 anhydrite layers, Zechstein (ZE) and Rotliegend (RO) seem to have the greatest effect on cluster centroid location whilst showing a different trend to velocity variations of other layers. For the Zechstein layer, especially in Figure 8, it is clear that an increase in velocity results in a shallower cluster centroid. Compared to shallower layers, the centroid parameters for the Z3, Z2 and Rotliegend layers have large variations whilst deviating from the trend of these shallower layers. Figure 8 also shows that a decrease in velocity of the Limburg Group, located below the initial focal depth of 3 km, has the same effect on the cluster centroid depth as a velocity increase in the RB & ZE and shallower layers, which are located shallower than the focal depth.

5.3 Ray theory

The behaviour of the cluster centroid location for small velocity variations within the source region has resulted in unexpected behaviour, i.e., a deviation from trends of other layers. Additionally, the trend for the cluster centroid depth for velocity variations in the Limburg Group is opposite to that of shallower layers. Because of this, and the dependence of *HypoDD* on ray theory, we have decided to investigate the effects of the velocity model on ray tracing. The ray paths are determined by shooting rays from an event at 3.0 km depth with increasing take-off angle with respect to the vertical, starting with upwards propagating rays. At each interface the ray encounters, the angle of propagation into the next layer is calculated with Snell's law,

$$n_1 sin\theta_1 = n_2 sin\theta_2, \tag{10}$$

where n_1 and n_2 are the slownesses (1/velocity) of the initial and next layer, respectively, θ_1 the angle of incidence and θ_2 the angle of the refracted ray with respect to the vertical. Continuation and travel time are tracked throughout the medium. Rays are not traced any further if the angle of incidence becomes equal or larger than the critical angle at an interface. When the angle of incidence becomes equal or larger than the critical angle, interface waves arise. Initially downgoing rays are allowed to reflect once in deeper layers to go upwards for them to turn. Initially upgoing rays are not allowed to reflect downwards at all. Additionally, calculations for downgoing rays that do not turn within the depth limit of the model are terminated once these rays reach the bottom limit. This bottom limit is set at 8.0 km depth.

The ray paths for an event at 3.0 km depth with the 12 layered velocity model are shown in Figure 9

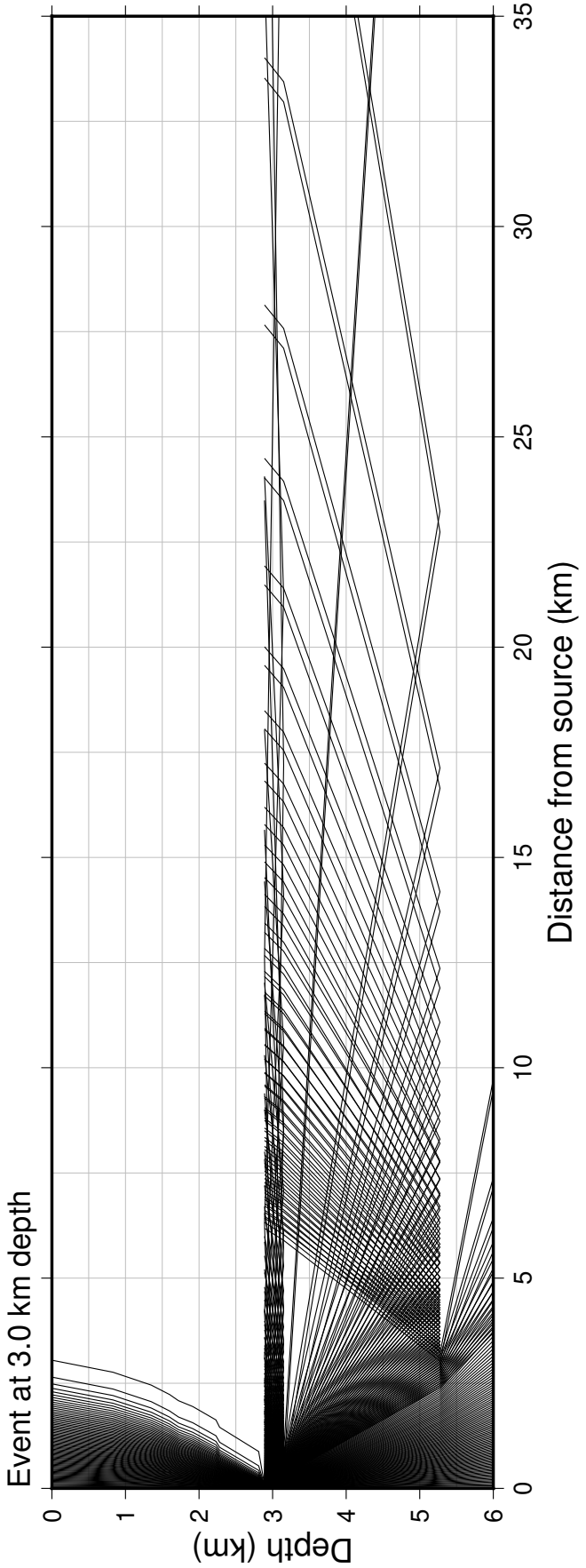

Figure 9: Ray paths for take-off angles that increase by 0.5° for a source at a hypocentral depth of 3.0 km for the 12 layered velocity model (Table C.2). Rays are not traced any further if the angle of incidence becomes equal or larger than the critical angle.

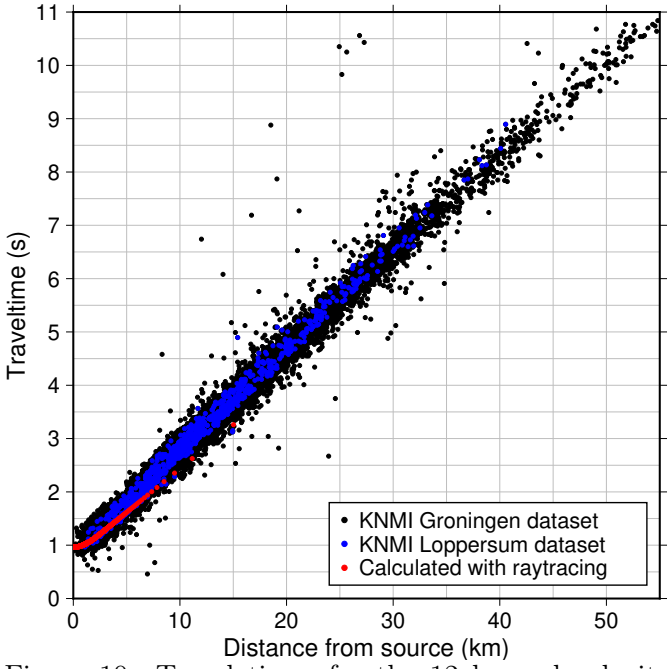

Figure 10: Travel times for the 12 layered velocity model, obtained by ray tracing for incident rays at 0.001° angle intervals, and the KNMI dataset for Groningen and Loppersum. The variation in travel times for the Groningen dataset is approximately 1 second for each epicentral distance.

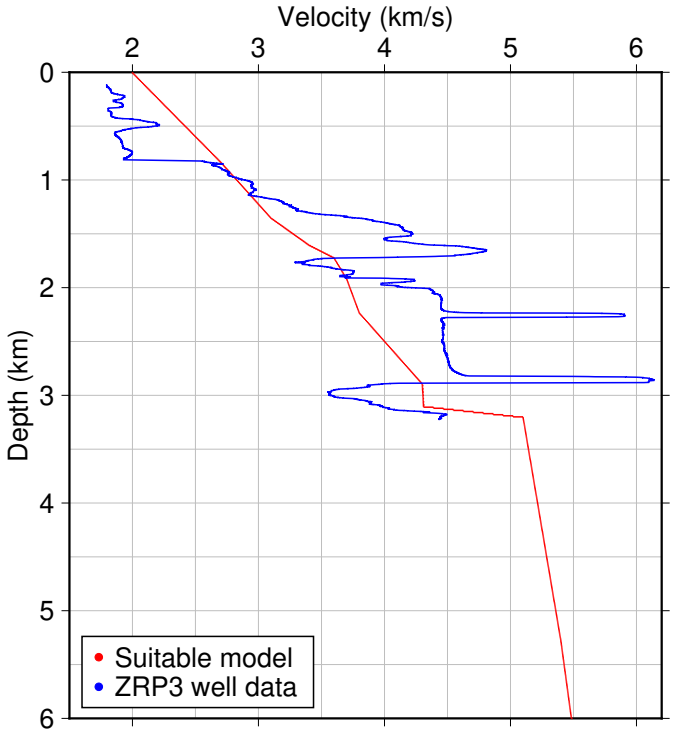

Figure 11: In red: velocity model for which the travel times match the KNMI dataset. In blue: velocity model from the ZRP3 well log.

for take-off angle intervals of 0.5°. None of the initial downgoing rays continue towards the surface because the velocity contrast between the high velocity cap rock and the directly surrounding velocity layers is too large and rays become interface waves. Only for incidence angles smaller than the critical angle, $\sin^{-1}(\frac{n_{max}}{n_{hypo}})$, where n_{hypo} denotes the slowness of the layer the event originates in and n_{max} the maximum slowness in shallower layers, the directly ascending ray manages to reach the surface. For larger angles, the ray path is trapped below the layer with n_{max}.

In order to use a velocity model to locate events, its travel time curve must fit the travel time data. For the 12 layered velocity model based on ZRP03, the fit between predicted and observed travel time is poor. The travel time from the source to the surface is too short for directly ascending rays and downgoing rays do not reach the surface (Figure 10). It should be noted that the variation in travel times at the same epicentral distances of the Groningen dataset is approximately 1 second, likely due to spatial variations in the seismic velocity structure and existing faults in the subsurface.

5.4 Suitable velocity model

The velocity contrast between the cap rock and its surrounding layers is too large, which results in trapped initially downgoing rays for the 12 layered velocity model. To circumvent this, we have found a better suited velocity model for which all initial descending rays, with exception of those rays that do not turn within the depth limit of the model, propagate to the surface. We generate this new velocity model so that the calculated travel times fit the trend of the KNMI travel time data. The choice is made to first find a velocity model with limited complexity. This velocity model is then smoothened by linear interpolation using 10 m thick (sub-)layers. A benefit is that rays are allowed to more gradually turn and change direction instead of a sudden reflection on a deeper interface. With trial and error a new velocity model is found that matches the travel time data.

To satisfy the condition that all downgoing rays reach the surface, besides those that do not turn within the model with max depth of 8 km, it is necessary to have a velocity model for which no low velocity layers are present shallower than the focal depth, i.e. the velocity has to increase with depth up to the event depth. Low velocity layers are allowed to be present deeper than the focal depth. However, for simplicity, we have chosen to not include any low velocity layers deeper than the source. Our final velocity model is plotted next to the ZRP3 well log in Figure 11 and listed in Table D.1. An overview of the resulting ray paths is shown by Figure 12 and the corresponding travel times by Figure 13. We can see that initially descending rays smoothly turn and propagate to the

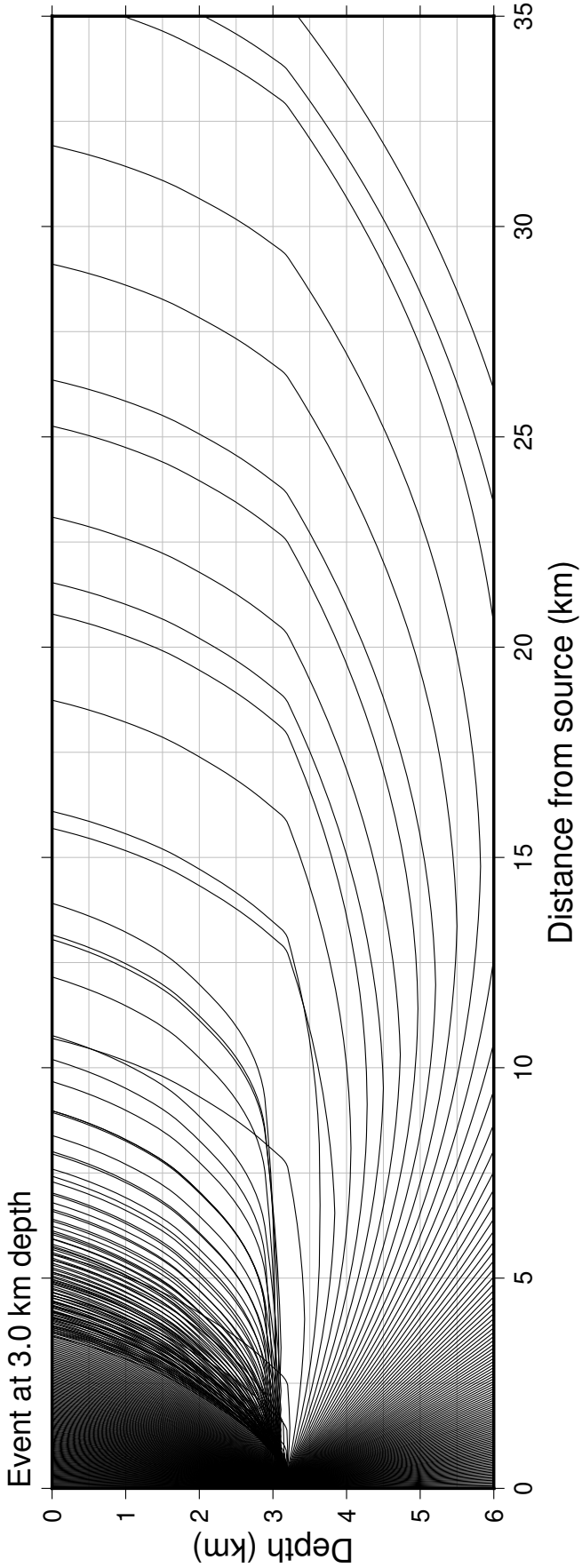

Figure 12: Ray paths for take-off angles that increase by 0.5° for a source at a hypocentral depth of 3.0 km for the final velocity model (Table D.1). Rays are not traced any further if the angle of incidence becomes equal or larger than the critical angle.

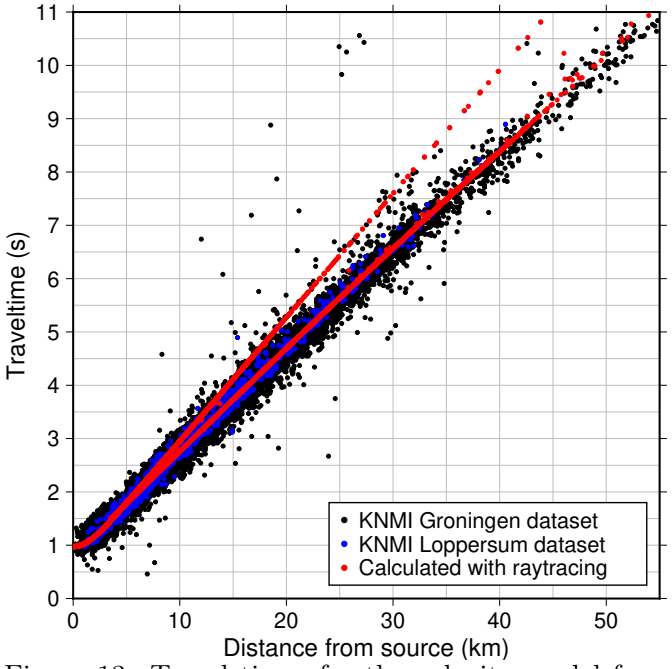

Figure 13: Travel times for the velocity model from Table D.1, obtained by ray tracing for incident rays at 0.001° angle intervals, and the KNMI dataset for Groningen and Loppersum. The variation in travel times for the Groningen dataset is approximately 1 second for each epicentral distance. There are two clear branches visible for the calculated travel times. These are direct upgoing rays that give first arrivals for the first 5 km epicentral distance and second arrivals for further distances and direct downgoing rays responsible for first arrivals for epicentral distances larger than 5 km.

surface. The first arrivals in Figure 13 show a good fit with both the Loppersum and the Groningen KNMI travel time data. The first arrivals consist of the directly ascending rays for the first 5.0 km and the descending rays for larger distances. At 5.0 km distance from the source a small triplication is visible (Figure 12).

5.5 Synthetic testing on depth location

We have synthetically tested relocation in *HypoDD* by changing the actual travel times listed by the KNMI to travel times found through ray tracing using the new velocity model. This is performed for the Loppersum area for events at their default depth of 3.0 km depth. Relocation results in a cluster centroid depth, i.e. average focal depth, of approximately 3.2 km depth. Because *HypoDD* relies on the notion that the interevent distance is much smaller than the source-station distance, and the first arrivals are composed of direct upgoing rays for the first 5.0 km distance, we removed arrivals with an epicenter location-receiver distance of 5.0 km. The removal of arrivals close to

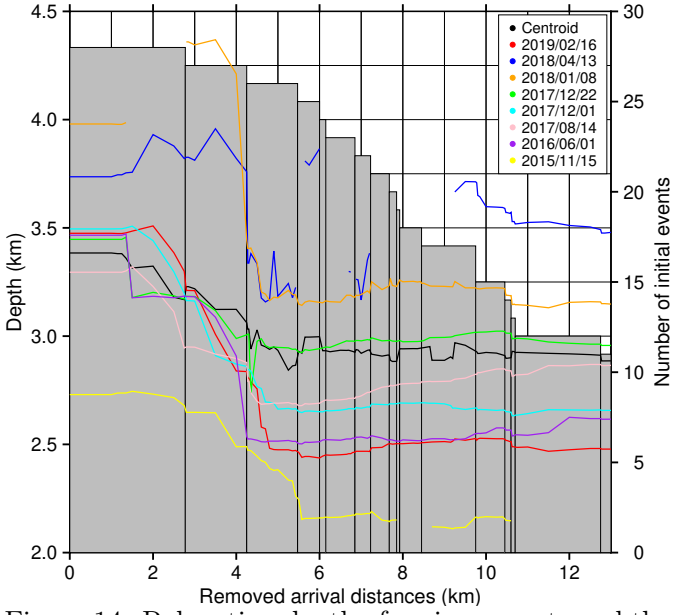

Figure 14: Relocation depth of various events and the centroid (black) for a range of arrival removal distances in the Loppersum region for the real KNMI data. The number of initial events used by *HypoDD* as a function of arrival removal distance is visualised by the gray bars.

the source location has resulted in a cluster centroid depth of 3.00 km, for which the largest deviation of an event is 11 m. We want to note that this is not an effect of damping. This suggests that the result produced by *HypoDD* is optimized by removing data that correspond to directly ascending rays from the dataset.

5.6 Relocation of the original datasets

In order to find the best value for which the arrivals have to be removed for the KNMI dataset, we track the relocation depth of various events (and the centroid) for a range of removed arrival distances in the Loppersum region (Figure 14). In general, events get relocated closer towards the surface for an increasing epicentral distance for which arrivals are removed. For larger distances, the event depth change stagnates and the focal depth remains relatively constant. The 2018/04/13, 2018/01/08 and 2015/11/15 events have a few gaps in their graph because they do not get relocated by *HypoDD* when some arrivals are removed. Even though nearly all events depths become relatively constant after the first 4 to 5.5 km of first arrivals are removed, the 2018/04/13 event has focal depth variations of up to 700 m.

The shallowest event (2015/11/15) coincides with the depth of the top of the anhydrite floater, located at approximately 2.25 km depth in the Loppersum area, for the removal of first arrivals up to 5.0 km epicentral distance. If arrivals for smaller epicentral distances are included in the dataset, this event relocates within the rock salt portion of the Zechstein. Because the rock salt undergoes ductile deformation when a stress is imposed (Carter et al., 1993), our events should only relocate within the anhydrite layers in the Zechstein. The removal of the first 5.0 km of arrivals is in agreement with the ideal distance found during synthetic testing.

To balance fitting the travel time differences with having realistic relative locations, we damp the solution. The damping parameter is chosen by means of L-curve optimization (Hansen, 2001), where on the x-axis we plotted 1/damping and RMS residual on the y-axis. We have tracked the RMS residual for a range of damping parameters, i.e., 1-50, for both the first and second iterative set per iteration. The region with the maximum curvature is the compromise between a solution dominated by the data errors and overdamping. For the first and second iterative set, the number of iterations is set to 2 and 3, respectively, as the residuals quickly converge. The L-curve plots can be found in Appendix E. The damping parameter is selected by visual inspection. For the Loppersum area, the damping is set to 25 and 20, respectively, for these iterative sets (Figure E.1, Figure E.2). For the Groningen area, 45 and 17, respectively, is chosen for the iterative sets (Figure E.3, Figure E.4).

A first-order approximation of the depth determination error is determined by varying the reservoir velocity. With this approximation, the largest depth variation between relocations with different reservoir velocities is considered the depth error. Calculated travel times for velocities between 3.8 and 4.7 km/s fit the KNMI travel time data (Figure 13). For these reservoir velocities, the first arrival filter for epicentral

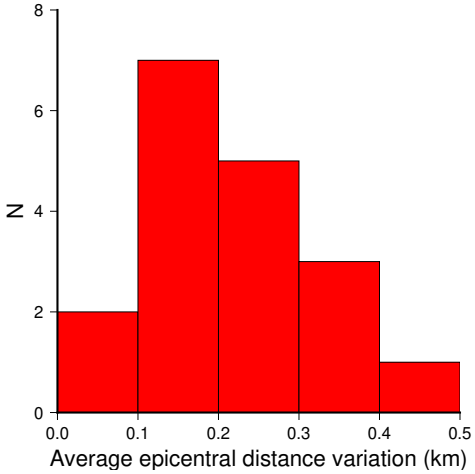

Figure 15: The average epicentral distance between the best relocation result (lowest RMS residual) and approximately 80 other *HypoDD* results that include different velocities and inversion parameter settings.

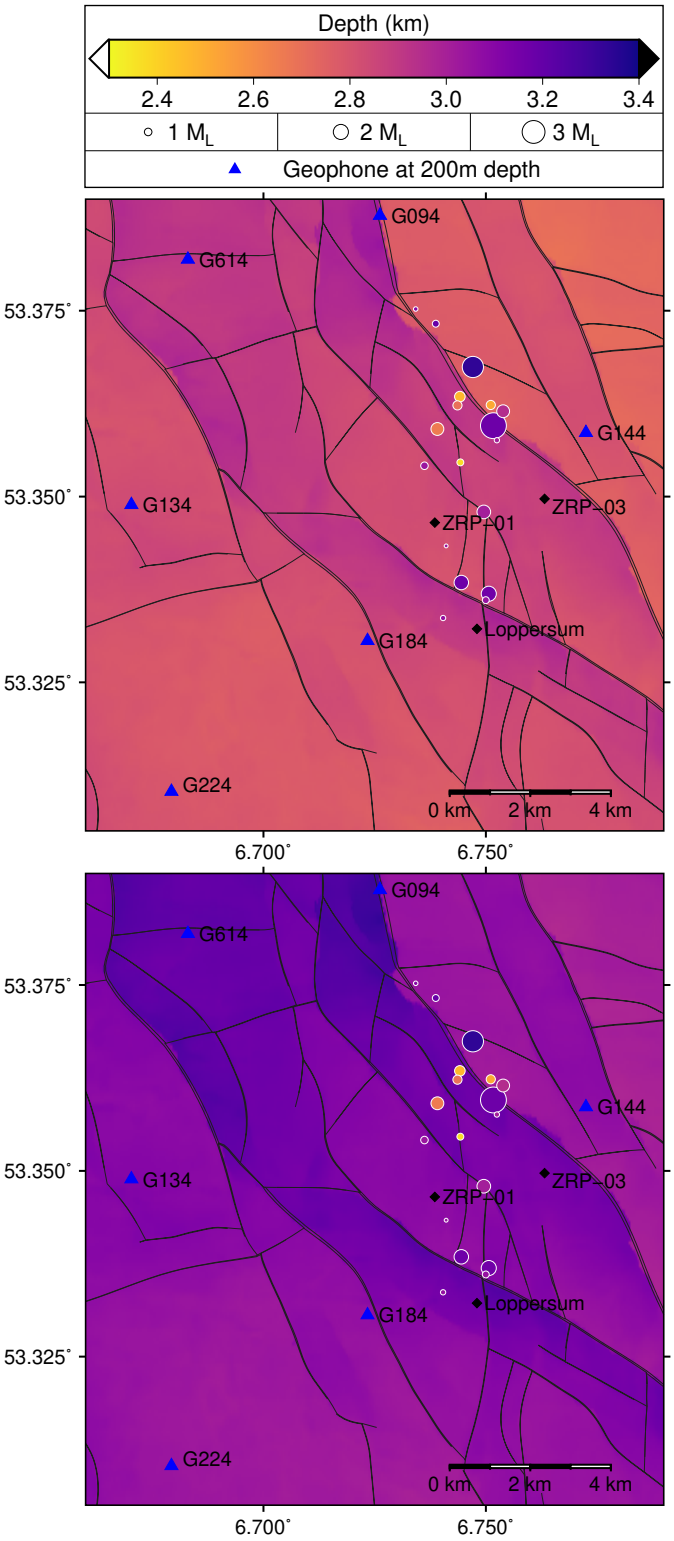

Figure 16: Hypocenter relocations for the Loppersum region. The background colouring indicates the depth of the top of the Rotliegend and Limburg Group formation, respectively. The gray lines indicate the faults at the top of the gas reservoir. The formation depth map and the fault map are from the NAM. Events are coloured based on focal depth and the size of the circles correspond to the earthquake magnitude.

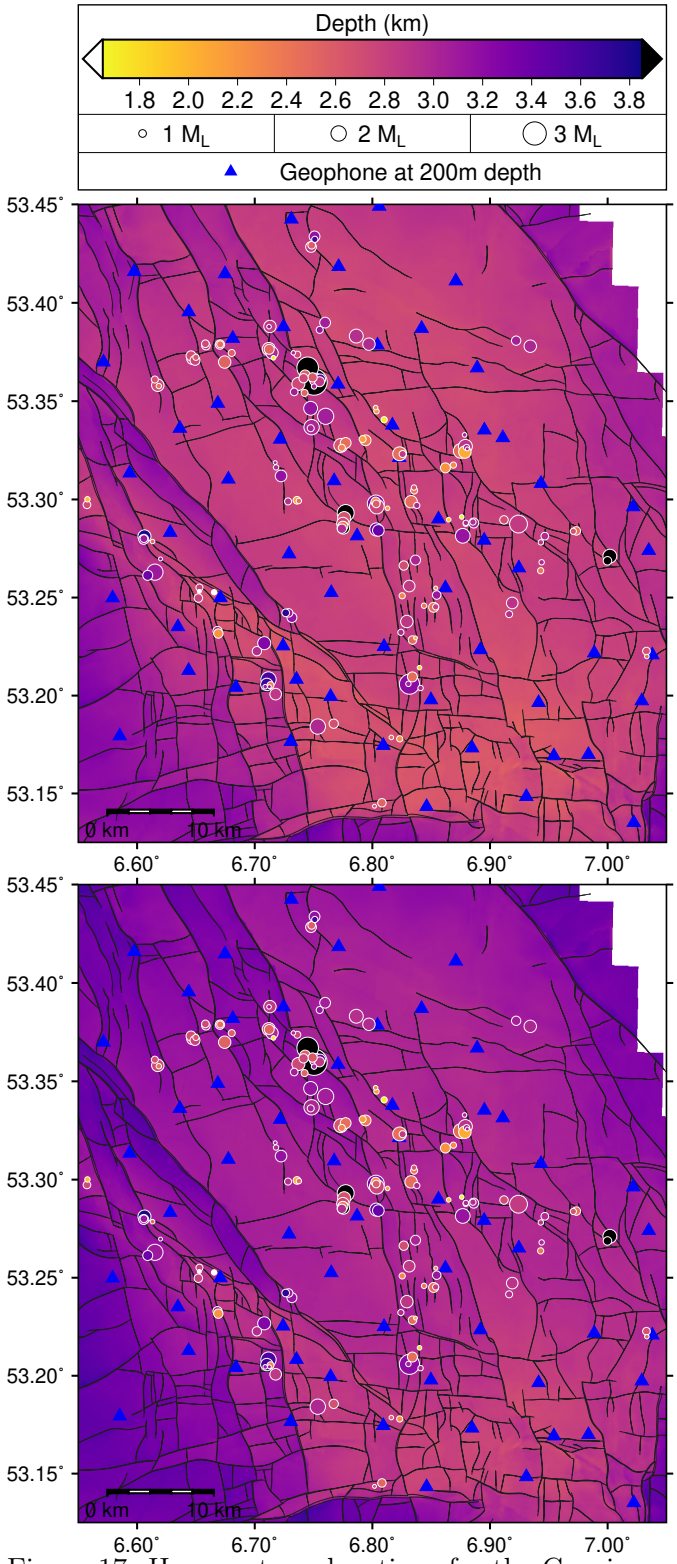

Figure 17: Hypocenter relocations for the Groningen region. The background colouring indicates the depth of the top of the Rotliegend and Limburg Group formation, respectively. The gray lines indicate the faults at the top of the gas reservoir. The formation depth map and the fault map are from the NAM. Events are coloured based on focal depth and the size of the circles correspond to the earthquake magnitude.

distances is applied again to get an overview of the general trends in event depths. These results are listed in Appendix F. The depth of the 2018/04/13 event behaves very unpredictably. The choice is made to not exclude this event from the dataset as the removal of odd behaving events results in odd behaviour of other events. As a result, the 2018/04/13 event is not considered for depth determination. Only for the velocities in the range of 4.1 to 4.4 km/s no deviations from the general trend are visible. Based on this range, a depth error of about 200 m is found.

Because there is no objective method to determine the accuracy of relocation, it is extremely difficult to quantify the uncertainty. The uncertainty in epicentral location is estimated by calculating the epicentral distance for each event individually between the *HypoDD* run with the lowest RMS residual and approximately 80 other runs. The latter includes runs with different velocity models, damping and arrival distance filters. With these distances, the standard deviation and average distance are calculated (Figure 15). We have found a standard deviation of 237.1 m with a maximum of 418.6 m (Figure 15).

The previously stated errors are specifically for the Loppersum region with our 1D velocity model. These errors may represent the achievable accuracy of *HypoDD* in the Groningen area when the relocation parameters are optimized. In reality, due to spatially varying formation depths and thus a laterally varying velocity model and faults in the subsurface, these errors are expected to be larger when relocation is applied on the entirety of the research area. For relocation on this larger scale, the same (pre-)inversion parameters, besides damping, are used.

The *HypoDD* parameters, used for relocation are listed in Table G.1 and Table G.2 for the Loppersum trial area and the Groningen region, respectively. The epicentral coordinates of events relocated with *HypoDD* and their initial location in the KNMI catalog can be found in Appendix H and Appendix I for the Loppersum and the Groningen datasets, respectively. The hypocenter depth for the KNMI database is not listed as it is set by default to 3.0 km. For the Loppersum area, the hypocenter locations compared to the top of the Rotliegend and Limburg Group are plotted in Figure 16. For the Groningen area, these are plotted in Figure 17.

In *HypoDD* events are only relocated relative to each other if they have enough links with other events within the research area. We have set this number of links to be 8. With the Loppersum dataset 18 out of 34 are relocated. For the Groningen dataset this is 159 out of 400. In the Loppersum region, west of ZRP1 and south of the town Loppersum, no events are relocated due to poor linkage. A majority of the events (13) are relocated in both the Rotliegend and Limburg Group. Their epicenters mostly coincide with mapped faults at the top of the Rotliegend (Figure 16). Events that do not correspond with faults mapped by the NAM are generally of smaller (< 1.0) magnitude. For the Groningen dataset, most events get relocated next to faults or directly on top of faults. It is visible that the focal depth of a large portion of the events is either shallower than the top of the Rotliegend or within the Limburg Group.

An overview of the final locations for events relocated with the Loppersum dataset and the Groningen dataset are given in Appendix H and Appendix I, respectively.

6 Discussion

We compare the event locations obtained through *HypoDD* with the locations in the KNMI catalog and events relocated by the EDT method (Spetzler and Dost, 2017). After a comparison with different methods, we continue with a few notes on faulting, the velocity model and ray tracing.

6.1 Method comparison

The results obtained with *HypoDD* for both the Loppersum and the Groningen regions are compared with the KNMI catalog locations and the locations found by Spetzler and Dost (2017) using the EDT method. Events are only shown if they are relocated by *HypoDD*.

6.1.1 *HypoDD* results versus KNMI locations in the Loppersum region

Figure 18 shows the difference in epicentral locations between the *HypoDD* results and KNMI catalog for the Loppersum area together with a cross section along A-A'. It is difficult to determine which method yields the most accurate event locations in the horizontal plane. In the vertical plane, the focal depth of all KNMI locations is 3.0 km. With *HypoDD*, the focal depth ranges from 2.4 km to 3.35 km depth. We interpret locations with an offset in cap rock, reservoir rock and gas source rock to be faults across those formations (Figure 18). Many events are horizontally directly located on or right next to inferred fault locations. Although 5 events get relocated within the Zechstein rock salt, their distance to either the cap rock or the anhydrite floater is typically less than 150 m, whereas our vertical uncertainty is 240 m. There-

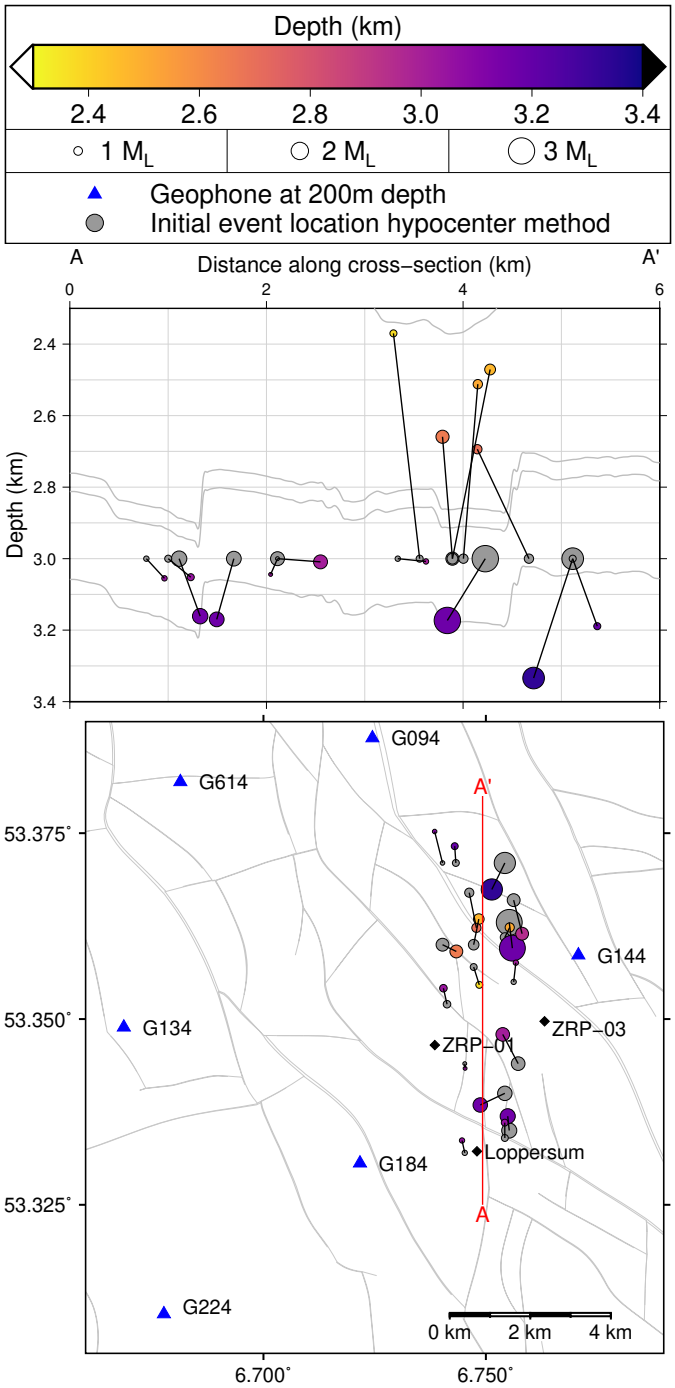

Figure 18: Comparison of the *HypoDD* relocation results (coloured) for the Loppersum region with the hypocenters of the KNMI catalog data (gray). Events that correspond to each other are connected with a black line. In map view (bottom panel), faults in the top of the Rotliegend formation are indicated with gray lines. Relocated events within 0.5 km of the cross section line A-A' are projected on the cross section (top panel). In the cross section, the gray lines represent the top of the anhydrite floater, cap rock, reservoir rock and gas source rock, respectively, from shallow to deep. The formation depth map and the fault map are from the NAM.

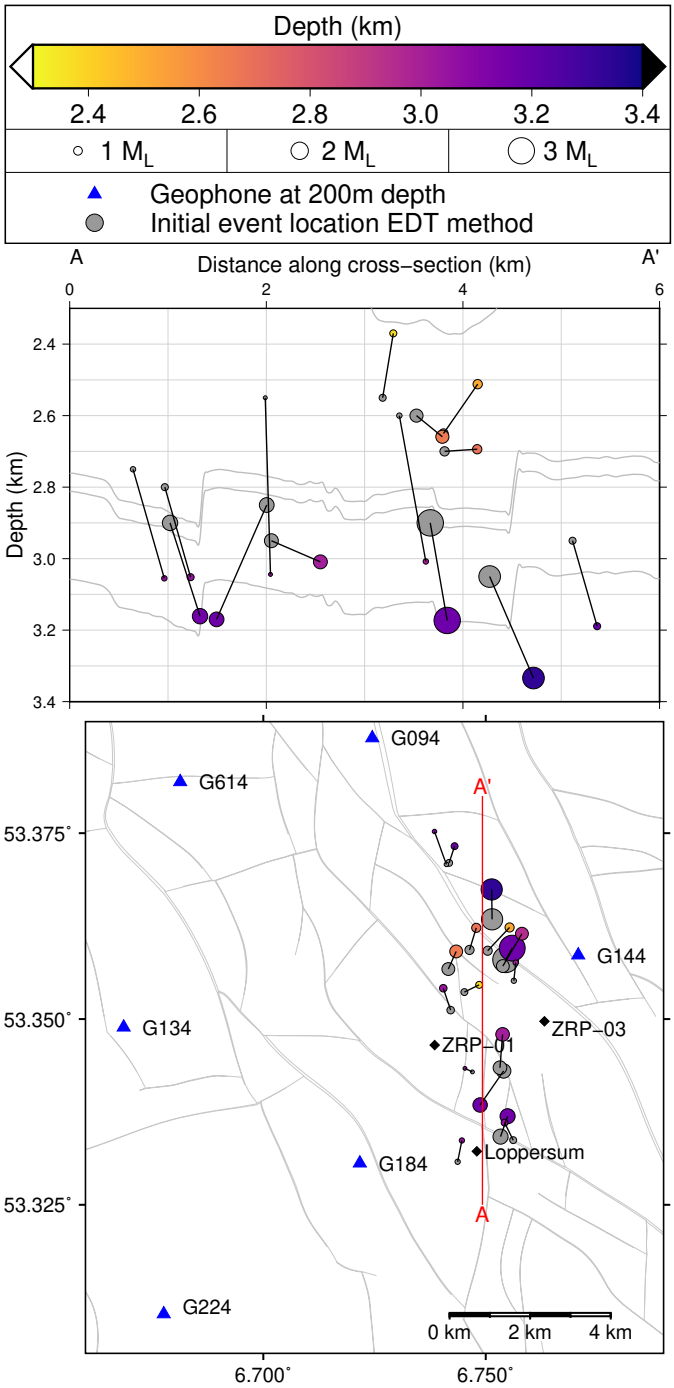

Figure 19: Comparison of the *HypoDD* relocation results (coloured) for the Loppersum region with the hypocenters of the EDT data (gray), by courtesy of Spetzler and Dost (2017). Events that correspond to each other are connected with a black line. In map view (bottom panel), faults in the top of the Rotliegend formation are indicated with gray lines. Relocated events within 0.5 km of the cross section line A-A' are projected on the cross section (top panel). In the cross section, the gray lines represent the top of the anhydrite floater, cap rock, reservoir rock and gas source rock, respectively, from shallow to deep. The formation depth map and the fault map are from the NAM.

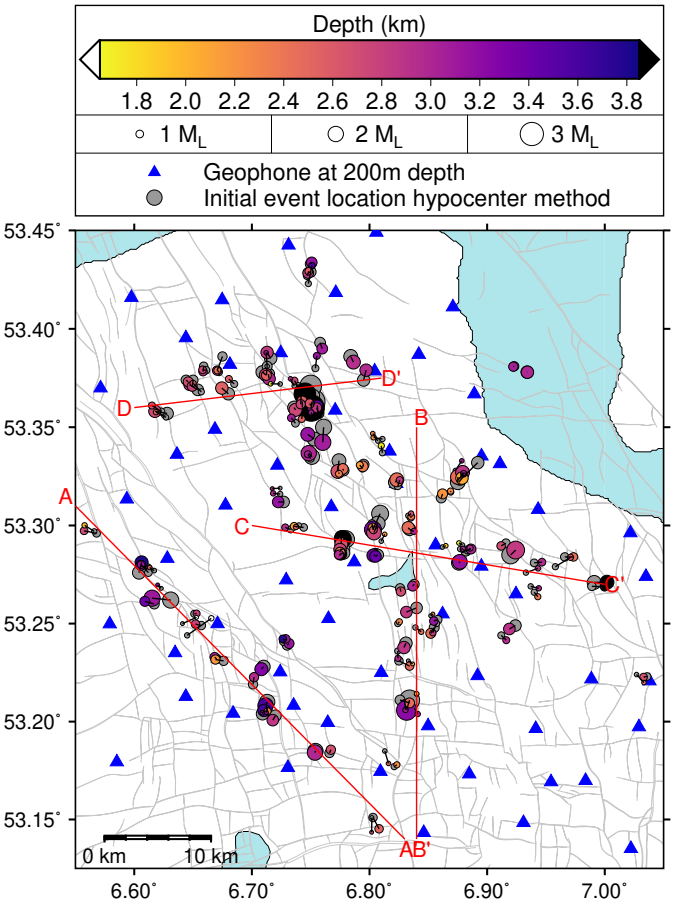

Figure 20: Comparison of the *HypoDD* relocation results (coloured) for the Groningen region with the epicenters of the KNMI catalog data (gray). Events that correspond to each other are connected with a black line. Faults in the top of the Rotliegend formation are indicated with gray lines. Relocated events within 1.5 km of the cross section line are projected on this cross section. Cross sections can be found in Figure 22.

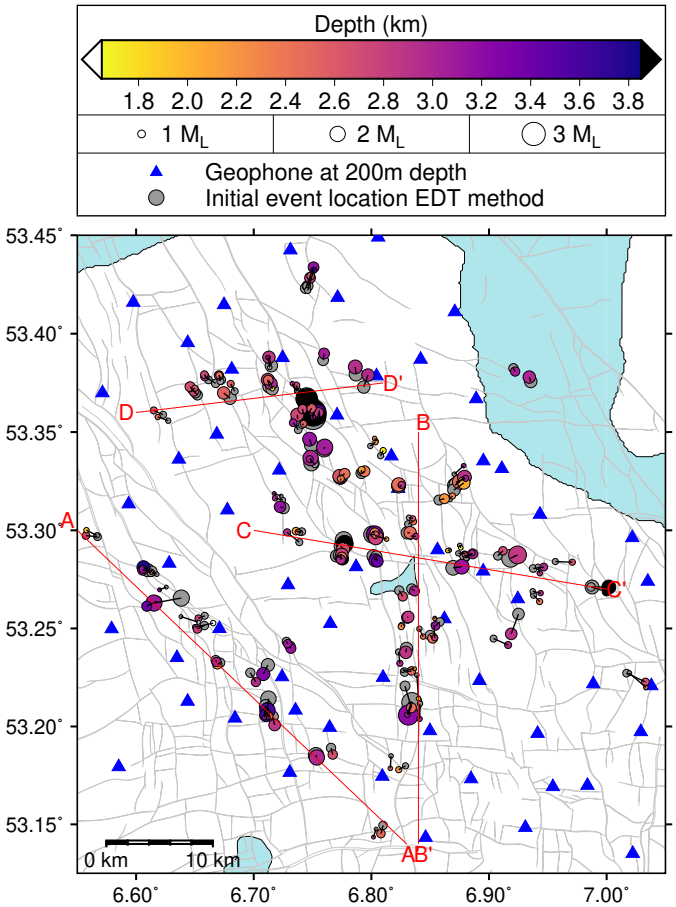

Figure 21: Comparison of the *HypoDD* relocation results (coloured) for the Groningen region with EDT data (gray), by courtesy of Spetzler and Dost (2017). Events that correspond to each other are connected with a black line. Faults in the top of the Rotliegend formation are indicated with gray lines. Relocated events within 1.5 km of the cross section line are projected on this cross section. Cross sections can be found in Figure 23.

fore, it is likely that these events are actually located within these anhydrite layers. Because the events relocated with *HypoDD* are on or next to faults, we are confident that relocation through the double-difference method, with our parameter settings and velocity model, yields more accurate hypocenter estimations than obtained by the *HYPOCENTER* method used by the KNMI.

6.1.2 *HypoDD* results versus EDT locations in the Loppersum region

The comparison between the results of Spetzler and Dost (2017) obtained by the EDT method and our *HypoDD* for the Loppersum area, along with cross section A-A', can be found in Figure 19. In the horizontal plane, more events are located directly on or next to faults compared to our results. However, events obtained by the double-difference method coincide better with faults in the vertical plane. With both methods events are relocated in the rock salt part of the Zechstein. Because these events get relocated towards the anhydrite floater and brittle deformation of rock salt is unlikely (Liang et al., 2012), both methods are in agreement that the anhydrite floater is potentially seismically active. There is no evidence of earthquakes in layers deeper than the gas reservoir rock for the EDT dataset in the Loppersum region. In contrast, relocations with the double-difference method suggest that these deeper events do exist.

Spetzler and Dost (2017) estimated the vertical location uncertainty in the EDT relocations to be between 100 and 400 m. They do not specifically provide horizontal uncertainties. However, note that for EDT Dost et al. (2017) indicated a horizontal uncertainty of 100 to 300 m and a vertical uncertainty of 300 m. Our estimated error, using *HypoDD*, is

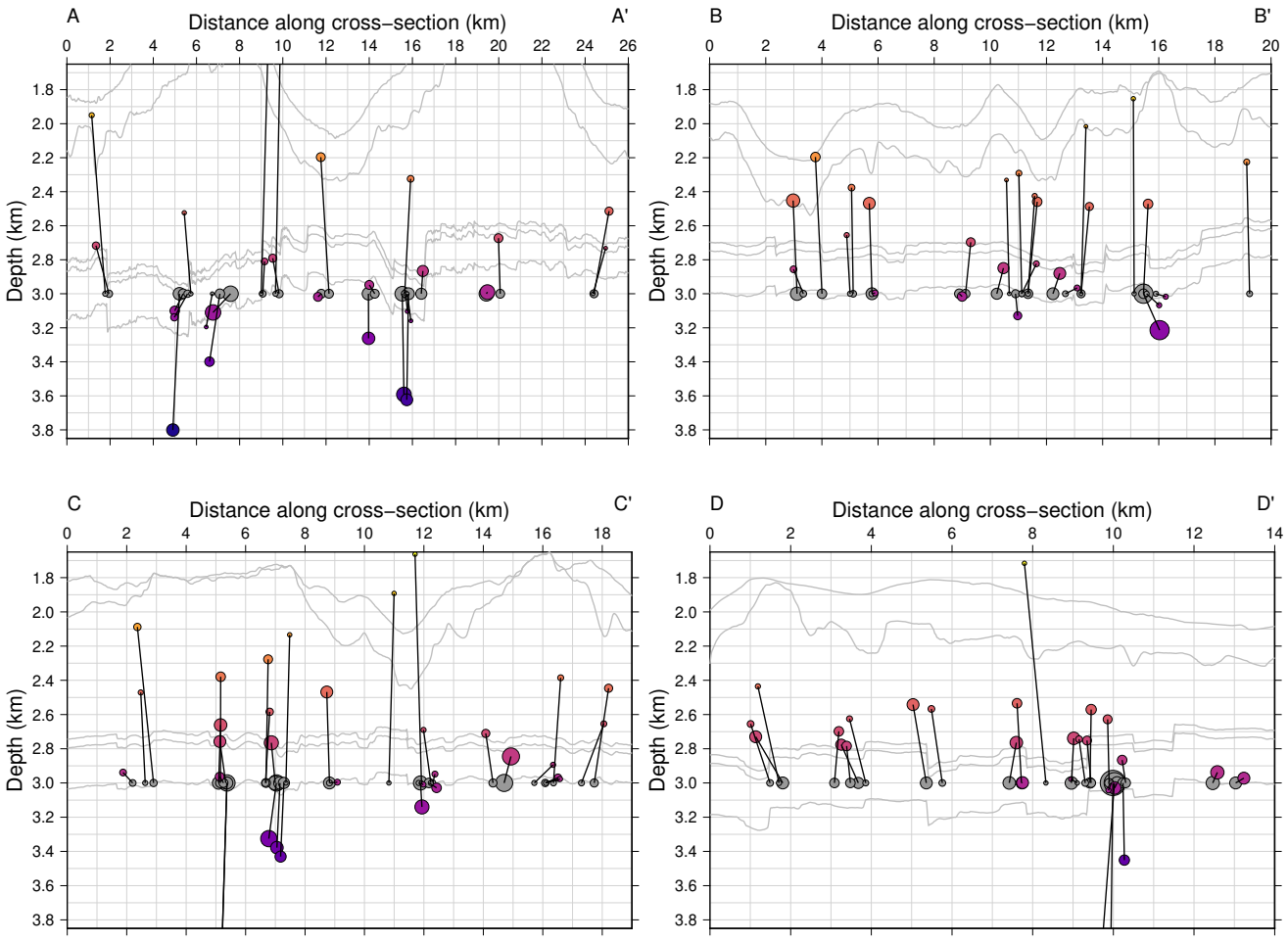

Figure 22: Cross sections from Figure 20 with the comparison between the *HypoDD* results (coloured) and the KNMI catalog data (gray). Events that correspond to each other are connected with a black line. The gray lines in the background from shallow to deep represent the depth op the top of the Zechstein, anhydrite floater, cap rock, reservoir rock and gas source rock, respectively. The formation depth map and the fault map are from the NAM.

240 m. When we take into consideration the horizontal and vertical errors for the EDT method and results obtained by *HypoDD*, some events are slightly too far apart, i.e. 50-100 m. This leads us to believe that the errors are underestimated. The method used by Spetzler and Dost (2017) to constrain vertical and horizontal error is by means of shifting the minimum of the misfit function based on the difference between calculated and observed travel times for all station pairs, which only serves as an indication of the uncertainty. Furthermore, we acknowledge that our estimation is a first-order approximation of the uncertainty.

6.1.3 Comparison of event locations in the Groningen region

The comparison in the horizontal plane between epicenters found using *HypoDD* and the KNMI catalog and *HypoDD* and the EDT method for the Groningen area can be found in Figure 20 and Figure 21, respectively. Their respective corresponding cross sections, to compare event location in the vertical plane, can be found in Figure 22 and Figure 23.

In the comparison of the horizontal plane between the KNMI locations and the events relocated with *HypoDD*, some events do not differ much in epicentral location, while others do within a short distance of each other. Additionally, in map view, both methods have a similar fit to the mapped faults at the top of the Rotliegend. Thus, there are no remarkable differences or similarities. The cross sections show that *HypoDD* relocates events in the rock salt part of the Zechstein, towards the anhydrite floater and in the gas source rock. This suggests that it is possible that the anhydrite floater and Limburg Group are seismically active. Especially in cross section D-D' it is clear that events get relocated either on faults or near to faults, indicating that these faults are active. Some

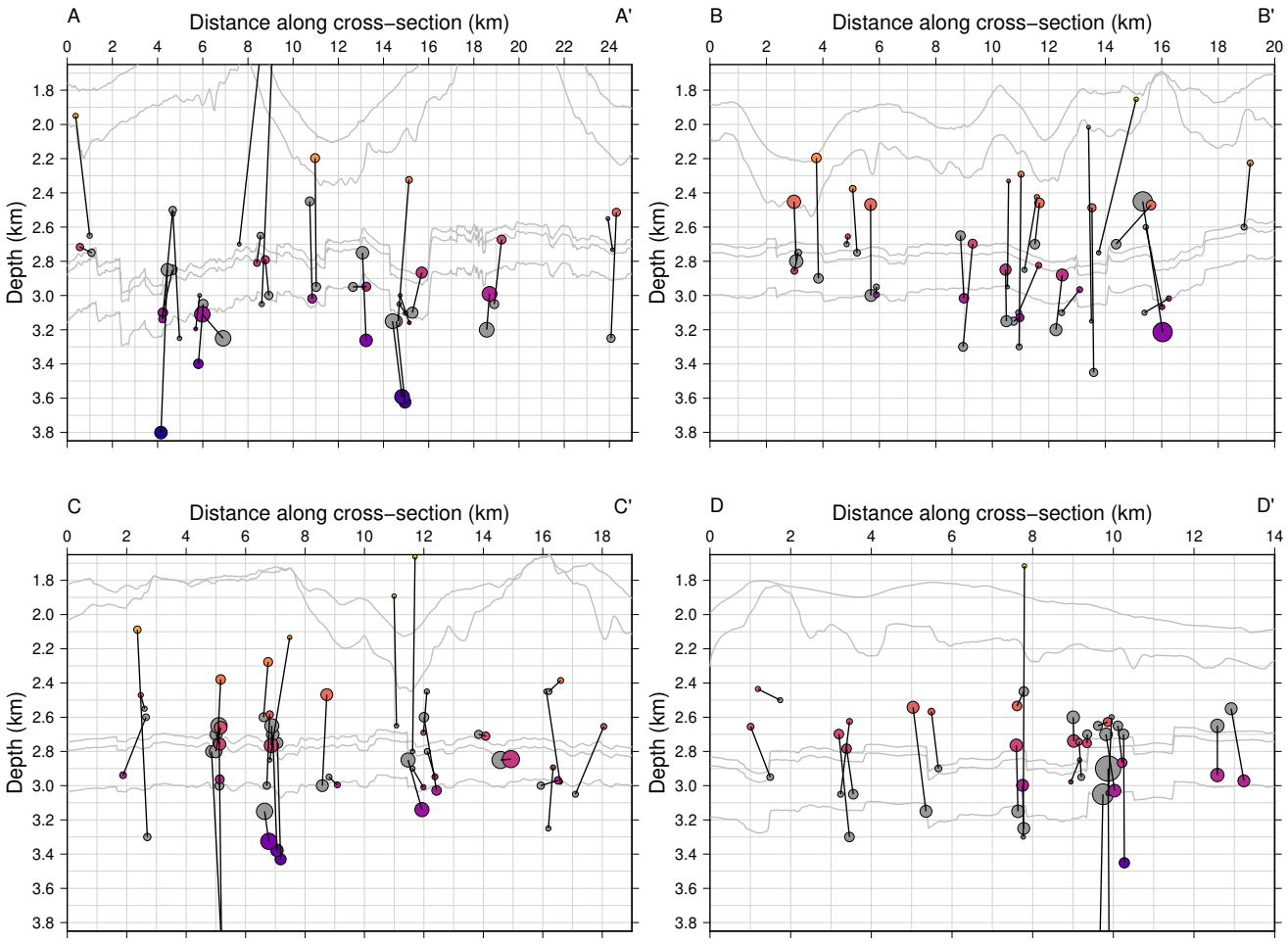

Figure 23: Cross sections from Figure 21 with the comparison between the *HypoDD* results (coloured) and the EDT relocations (gray). Events that correspond to each other are connected with a black line. The gray lines in the background from shallow to deep represent the depth of the top of the Zechstein, anhydrite floater, cap rock, reservoir rock and gas source rock, respectively. The formation depth map and the fault map are from the NAM.

events get relocated above the top of the Zechstein formation, generally shallower than 1.8 km depth, in A-A', C-C' and D-D' and a few events get relocated deep within the Limburg Group formation, generally deeper than 3.7 km depth, in the same cross sections (Figure 22). The same trends are visible as the Loppersum dataset, i.e. a seismically active anhydrite floater and gas source rock with faulting that continues within this gas source rock. Because of this, we consider our *HypoDD* locations for the Groningen region to be better than the KNMI catalog. Especially because focal depth is not fixed at 3.0 km depth anymore.

Compared to the EDT method, events relocated with *HypoDD* are located further outwards from the centre of the region, which we define as longitude 6.80° and latitude 53.30° (Figure 21). We are uncertain if this is due to the limited number of stations beyond the edges of the gas field, resulting in significant azimuthal gaps or if the EDT method prefers to relocate events towards the center of this region. Closer to the centre, epicentral locations do not vary much between both methods. In the vertical plane, events rarely get located at the same focal depth. All cross sections (Figure 23) show that events that relocate within the gas source rock or bottom of the Rotliegend formation with the EDT method get relocated shallower with the double-difference method, often at the cap rock or within the Zechstein formation and vice versa.

Between the EDT method and *HypoDD*, it is difficult to say which method yields more accurate relocation results. Under the constraints that the subsurface velocity has to increase with depth up to the reservoir depth, while satisfying the travel time curve, and the removal of direct upgoing rays from the hypocenter, *HypoDD* has proved itself to be a good and reliable relocation program within the Lopper-

sum region. Uncertainties are expected to be quite a bit larger for relocations within the spatial dimensions of the larger Groningen area compared to those in the Loppersum trial area due to lateral variations in the velocity model. These lateral variations are also indicated by the travel time curve (Figure 13) for the KNMI Groningen dataset as for every source-receiver distance the travel time range is approximately 1 second. For smaller areas, where the 1D velocity model can be used as a valid approximation, i.e. a limited amount of faults and velocity heterogeneities, events relocated with the double-difference method line up better with faults in the subsurface compared to the EDT method. Additionally, because of similar uncertainties, we consider the double-difference method to yield comparable results to the EDT method.

6.2 Fault activity

We have seen that some events, especially those with smaller magnitudes, do not directly correspond to faults mapped by the NAM (Figure 16). By ant tracking, Kortekaas and Jaarsma (2017) have shown that many more faults, besides those listed by the NAM, do exist in the subsurface of Groningen. Kortekaas and Jaarsma (2017) determined that the average dip of the fault plane in the subsurface of Groningen is between 65° and 90°. Because events deeper than the reservoir often correspond to faults in the reservoir rock, it is expected that these faults continue to deeper subsurface formations and are seismically active.

6.3 Velocity model and ray tracing

An assumption made by *HypoDD* is that stations are located at the surface, i.e. at a depth of 0 m. We have used geophones located at 200 m depth within the Groningen area because these have a good signal to noise ratio, which results in better P-wave arrival picks for events. In our methodology we have not compensated for this, e.g., by removing the top 200 m of the velocity model. Because travel time differences are attributed to relative event locations in the source region, the effects on our results of having geophones at 200 m depth instead of the surface may be limited. While propagating, the steepness, i.e. angle with respect to the vertical, of rays constantly changes. Rays arriving at 200 m depth are less steep compared to rays arriving at the surface. This results in slightly different ray paths and arrival locations. Because this consistently is not compensated for, we believe that it may have small effects on event locations. We speculate that compensating for these geophones at depth would lead to a decrease in the uncertainty of up to 10 meters.

For areas with large lateral variations in the velocity structure, major improvements to the accuracy can be made. This can be done by either allowing ray tracing for a 3D velocity model or by subdividing the Groningen area in many smaller sub-areas, such as the Loppersum region in this study. A 3D velocity model may be challenging to implement and in the meantime it is also computationally far more demanding. Additionally, it may be difficult to combine a 3D velocity model with the increasing velocity with depth constraint. As we have seen, relocation results are heavily dependent on the input velocity model. Subdividing the Groningen region in smaller areas requires good 1D velocity model approximations for each sub-area. It is important to have a decent linkage between events and to let these sub-areas overlap with one another. This overlap would be required to cross-check for events that lie at edges with other regions if the focal depth and the epicentral location matches. If hypocenters at edges are similar in two regions, these regions can be combined to form a larger area. We expect that the uncertainty for this combined region would be smaller compared to relocation for this entire region at once.

One of the limitations of *HypoDD* is that calculated travel times are based on ray tracing. Ray theory is a high frequency approximation to the solution of the wave equation. It does describe the propagation of a ray throughout, a preferably, smooth medium through reflections and refractions. However, due to the high frequency approximation, phenomena such as diffraction, destructive and constructive interference and scattering on small scale features can not be represented through ray theory. Ideally, in order to capture all effects of the subsurface on the propagation from the source to the receiver in a medium, entire waveforms are used.

Because Waldhauser and Ellsworth (2000) indicates that hypocenter locations become more accurate with the inclusion of waveform cross-correlation methods, we could include cross-correlation data in the Groningen region and compare it with our current results in further research.

7 Conclusion

The densification of the geophone network in Groningen since 2014 has resulted in a large increase of the available data and the number of events and also in smaller azimuthal gaps. For *HypoDD* this allows for better linkage between events, and thus better results.

We have seen that under the constraint of velocity increase with depth up to the gas reservoir depth, while the corresponding travel times fit the actual data, and with the removal of arrivals within 5 km of the epicenter location, relocation with the double-difference method in relatively small areas proved itself to be viable. Although *HypoDD* has its limitations, i.e. a 1D velocity model and travel time calculation with ray tracing, it shows potential. In the Loppersum region we have managed to achieve an accuracy of approximately 240 m in both the horizontal and vertical planes. For this same region, our results indicate that both anhydrite layers, i.e. the floater and the cap rock, the reservoir and the gas source rock are seismically active. Compared to the KNMI catalog obtained with the HYPOCENTER method, we are confident that our double-difference relocations are better because focal depths are not fixed anymore and events get relocated towards faults in the subsurface. With respect to the EDT method, similar uncertainties have been found as well as an agreement in formations that likely are seismically active. Our results show that it is likely that faults in the cap rock and/or Rotliegend formation continue within the Limburg Group formation. For relocation for the Groningen area, we think that our errors likely are larger than those obtained for the Loppersum dataset because of large lateral velocity variations and subsurface heterogeneities. In order to obtain results with lower uncertainties for the Groningen dataset, subdividing the Groningen area in smaller overlapping areas with individual 1D velocity models would be beneficial.

Acknowledgements

I would first like to thank my thesis supervisors Hanneke Paulssen and Matthew Herman for their constructive feedback and suggestions, inspiring discussions and thoughts. I am grateful to Wen Zhou, Elmer Ruigrok, the KNMI and the NAM for providing useful datasets. I would also like to thank Marius Wouters, Maurits Beudeker and Boris Gesbert for their constructive feedback during the research and writing process. Last but not least, I want to express my gratitude to my parents and my girlfriend for their unfailing support and encouragement, both throughout my years of studying and during this thesis.

References

Akbar, M. F. (2018). Subsurface Reflection and Transmission Response Estimation by Seismic Interferometry Using Deep Borehole Data at Groningen. Master's thesis. Retrieved from https://dspace.library.uu.nl/handle/1874/367996.

Billings, S., Kennett, B. L., and Sambridge, M. S. (1994). Hypocentre location: genetic algorithms incorporating problem-specific information. *Geophysical Journal International*, 118(3):693–706.

Carter, N., Horseman, S., Russell, J., and Handin, J. (1993). Rheology of rocksalt. *Journal of Structural Geology*, 15(9-10):1257–1271.

De Jager, J. (2007). Geological development. *Geology of the Netherlands. Royal Netherlands Academy of Arts and Sciences, Amsterdam*, 5:26.

de Jager, J. and Visser, C. (2017). Geology of the Groningen field–an overview. *Netherlands Journal of Geosciences*, 96(5):s3–s15.

Dost, B., Ruigrok, E., and Spetzler, J. (2017). Development of seismicity and probabilistic hazard assessment for the Groningen gas field. *Netherlands Journal of Geosciences*, 96(5):s235–s245.

Font, Y., Kao, H., Lallemand, S., Liu, C.-S., and Chiao, L.-Y. (2004). Hypocentre determination offshore of eastern Taiwan using the Maximum Intersection method. *Geophysical Journal International*, 158(2):655–675.

Geiger, L. (1910). Herdbestimmung bei Erdbeben aus den Ankunftszeiten. *Nachrichten von der Gesellschaft der Wissenschaften zu Göttingen, Mathematisch-Physikalische Klasse*, 1910:331–349.

Geluk, M. C. (2007). Triassic. *Geology of the Netherlands. Royal Netherlands Academy of Arts and Sciences, Amsterdam*, 85:106.

Hansen, P. (2001). The L-curve and its use in the numerical treatment of inverse problems. Computational Inverse Problems in Electrocardiology. *Advances in Computational Bioengineering*, 5:119.

Jagt, L., Ruigrok, E., and Paulssen, H. (2017). Relocation of clustered earthquakes in the Groningen gas field. *Netherlands Journal of Geosciences*, 96(5):s163–s173.

KNMI (2019a). KNMI FDSN Event Web Service. http://rdsa.knmi.nl/fdsnws/event/1/. Last accessed 12/02/2019.

KNMI (2019b). Nederlandse stations. https://www.knmi.nl/nederland-nu/seismologie/stations. Last accessed 04/04/2019.

Kombrink, H. (2008). *The Carboniferous of the Netherlands and surrounding areas; a basin analysis. Geologica Ultraiectina (294)*. Departement Aardwetenschappen.

Kortekaas, M. and Jaarsma, B. (2017). Improved definition of faults in the Groningen field using seismic attributes. *Netherlands Journal of Geosciences*, 96(5):s71–s85.

Liang, W., Zhang, C., Gao, H., Yang, X., Xu, S., and Zhao, Y. (2012). Experiments on mechanical properties of salt rocks under cyclic loading. *Journal of Rock Mechanics and Geotechnical Engineering*, 4(1):54–61.

Lienert, B. R., Berg, E., and Frazer, L. N. (1986). HYPOCENTER: An earthquake location method using centered, scaled, and adaptively damped least squares. *Bulletin of the Seismological Society of America*, 76(3):771–783.

Menning, M., Katzung, G., and Lutzner, H. (1988). Magnetostratigraphic Investigations in the Rotliegendes (300-252 MA) of Central-Europe. *Zeitschrift fur geologische Wissenschaften*, 16(11-12):1045.

Mosteller, F. and Tukey, J. W. (1977). Data analysis and regression: a second course in statistics. *Addison-Wesley Series in Behavioral Science: Quantitative Methods*.

NAM (2011). Aardgas in Nederland. https://web.archive.org/web/20110809080933/http://www.nam.nl/home/content/nam/general/natural_gas_netherlands/. Last accessed 15/10/2019.

NAM (2019). NAM interactive kaart. https://nam-feitenencijfers.data-app.nl/embed/component/?id=interactieve-kaart. Last accessed 16/04/2019.

Paige, C. C. and Saunders, M. A. (1982). LSQR: An algorithm for sparse linear equations and sparse least squares. *ACM Transactions on Mathematical Software (TOMS)*, 8(1):43–71.

Romijn, R. (2017). Groningen Velocity Model 2017 - Groningen full elastic velocity model September 2017. https://nam-feitenencijfers.data-app.nl/download/rapport/9a5751d9-2ff5-4b6a-9c25-e37e76976bc1?open=true. Last accessed 11/03/2019.

Spetzler, J. and Dost, B. (2017). Hypocentre estimation of induced earthquakes in Groningen. *Geophysical Journal International*, 209(1):453–465.

Theunissen, T., Font, Y., Lallemand, S., and Gautier, S. (2012). Improvements of the maximum intersection method for 3D absolute earthquake locations. *Bulletin of the Seismological Society of America*, 102(4):1764–1785.

TNO (2019). DINOloket, Data and Information of the Dutch Subsurface. https://www.dinoloket.nl/en. Last accessed 11/03/2019.

Van Adrichem Boogaert, H. A. and Kouwe, W. F. (1997). Stratigraphic Nomenclature of the Netherlands, Revision and Update by RGD and NOGEPA, Meded. *Rijks Geol. Dienst*, 50.

Van Gent, H., Urai, J. L., and De Keijzer, M. (2011). The internal geometry of salt structures–A first look using 3D seismic data from the Zechstein of the Netherlands. *Journal of Structural Geology*, 33(3):292–311.

Van Wijhe, D. H. (1981). The Zechstein 2 Carbonate exploration in the eastern Netherlands-Proc. In *Int. Symp. Central European Permian, Jablonna*, volume 1978, pages 574–586.

Waldhauser, F. (2001). hypoDD–A Program to Compute Double-Difference Hypocenter Locations (hypoDD version 1.0-03/2001). *US Geol. Surv. Open File Rep., 01*, 113.

Waldhauser, F. and Ellsworth, W. L. (2000). A double-difference earthquake location algorithm: Method and application to the northern Hayward fault, California. *Bulletin of the Seismological Society of America*, 90(6):1353–1368.

Waldhauser, F., Ellsworth, W. L., and Cole, A. (1999). Slip-parallel seismic lineations on the northern Hayward fault, California. *Geophysical Research Letters*, 26(23):3525–3528.

Appendix A *ph2dt* and *HypoDD* parameters

Table A.1: Description and units for *ph2dt* input parameters.

Parameter	Parameter description	Unit
MINWGHT	Minimum weight for picks (0-1).	–
MAXDIST	Maximum distance between an event pair and a receiver	km
MAXSEP	Maximum distance between hypocenters of event pairs	km
MAXNGH	Maximum number of neighbours	–
MINLINK	Minimum number of links to define a neighbour	–
MINOBS	Minimum number of observations	–
MAXOBS	Maximum number of observations	–

Table A.2: Description and units for *HypoDD* input parameters.

Parameter	Parameter description	Unit
IDAT	Data type: 1 = cross correlation data, 2 = catalog data, 3 = cross-correlation and catalog data	–
IPHA	Phase picks used: 1 = P-waves, 2 = S-waves, 3 = P-& S-Waves	–
DIST	Maximum cluster centroid-receiver distance	km
OBSCC	Minimum number of cross correlation links per event pair	–
OBSCT	Minimum number of catalog links per event pair	–
ISTART	Initial locations of events: 1 = at cluster centroid, 2 = at catalog locations	–
ISOLV	The solver to use: 1 = SVD, 2 = LSQR	–
NSET	Number of iterative sets	–
NLAY	Number of layers in the velocity model	–
RATIO	V_p/V_s ratio (max 1 ratio)	–
TOP	Depth of the top of each layer	km
VEL	Velocities of each layer	km/s
CID	Cluster ID to be relocated	–
NITER	Number of iterations with the defined weighting parameters	–
WTCCP	P-wave weights for cross correlation data	–
WTCCS	S-wave weights for cross correlation data	–
WRCC	Residual cutoff threshold α for cross correlation data (equation (8))	s
WDCC	Maximum distance c between event pairs for cross correlation data (equation (9))	km
WTCTP	P-wave weights for catalog data	–
WTCTS	S-wave weights for catalog data	–
WRCT	Residual cutoff threshold α for catalog data (equation (8))	s
WDCT	Maximum distance c between event pairs for catalog data (equation (9))	km
DAMP	Damping parameter, only used for LSQR solver	–

Appendix B FDSN query parameters

Table B.1: FDSN query parameters used for each dataset for the entirety of Groningen to request data from the KNMI web service.

Dataset	Lon. (min/max)	Lat. (min/max)	M_L	Start date	End date
Pre-2014	6.45°/7.20°	53.00°/53.55°	0.85	01/01/1995	23/10/2014
Post-2014	6.45°/7.20°	53.00°/53.55°	0.45	23/10/2014	01/04/2019
Combined	6.45°/7.20°	53.00°/53.55°	0.85	01/01/1995	23/10/2014
	6.45°/7.20°	53.00°/53.55°	0.45	23/10/2014	01/04/2019

Table B.2: FDSN query parameters used for each dataset for the Loppersum trial area to request data from the KNMI web service.

Dataset	Lon. (min/max)	Lat. (min/max)	M_L	Start date	End date
Pre-2014	6.675°/6.754°	53.320°/53.371°	0.85	01/01/1995	23/10/2014
Post-2014	6.675°/6.754°	53.320°/53.371°	0.45	23/10/2014	01/04/2019
Combined	6.675°/6.754°	53.320°/53.371°	0.85	01/01/1995	23/10/2014
	6.675°/6.754°	53.320°/53.371°	0.45	23/10/2014	01/04/2019

Table B.3: The sizes of the datasets after pre-processing the complete datasets as requested from the KNMI with the query parameters listed in Table B.1 and Table B.2.

Dataset	Region	Nr. of events	Nr. of arrivals	Nr. of different stations
Pre-2014	Loppersum	74	334	8
Post-2014	Loppersum	34	881	77
Combined	Loppersum	108	1215	77
Pre-2014	Groningen	667	2694	15
Post-2014	Groningen	400	9015	83
Combined	Groningen	1067	11709	83

Appendix C Input parameters 12 layered Loppersum model

Table C.1: Parameter settings for *ph2dt*.

Parameter	Value
MINWGHT	0
MAXDIST	200
MAXSEP	10
MAXNGH	42
MINLINK	1
MINOBS	1
MAXOBS	100

Table C.2: 12 layered velocity model.

Depth of layer top (km)	Velocity (km/s)
0.0	2.0
0.83	3.1
1.35	4.1
1.6	4.75
1.72	3.55
1.915	4.35
2.23	5.9
2.28	4.5
2.81	6.1
2.89	3.9
3.15	4.25
5.275	5.3

Table C.3: Parameter settings for *HypoDD* yielding the lowest RMS residual output for the 12 layered Loppersum velocity model. It should be noted that cross-correlation parameter settings are left out, i.e. 0 if pre-inversion parameter and −9 if inversion parameter. The number after the parameter denotes which iterative set it belongs to.

Parameter	Value
IDAT	2
IPHA	3
DIST	55
OBSCT	8
ISTART	2
ISOLV	2
NSET	2
NITER1	4
WTCTP1	1
WTCTS1	−9
WRCT1	−9

Parameter	Value
WDCT1	−9
DAMP1	25
NITER2	6
WTCTP2	1
WTCTS2	−9
WRCT2	3
WDCT2	8
DAMP2	25
NLAY	12
RATIO	1.73
CID	0

Appendix D Optimal velocity model

Table D.1: Velocity model fitting the travel time curve of the raw data. This velocity model is smoothened by using the velocity gradients between two subsequent velocities at depth to linearly interpolate for 10 meter thick layers.

Depth (km)	**Velocity (km/s)**
0.0	2.0
0.83	2.7
1.35	3.1
1.6	3.4
1.72	3.6
1.915	3.7
2.23	3.8
2.89	4.3
3.1	4.31
3.2	5.1
5.275	5.4
7.0	5.6

Appendix E L-curve optimization

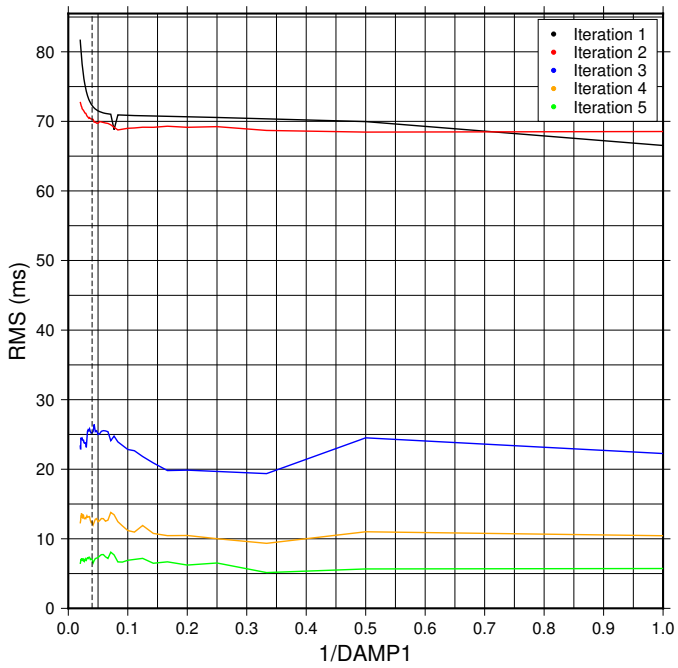

Figure E.1: L-curve optimization for the first iterative set in *HypoDD* for Loppersum.

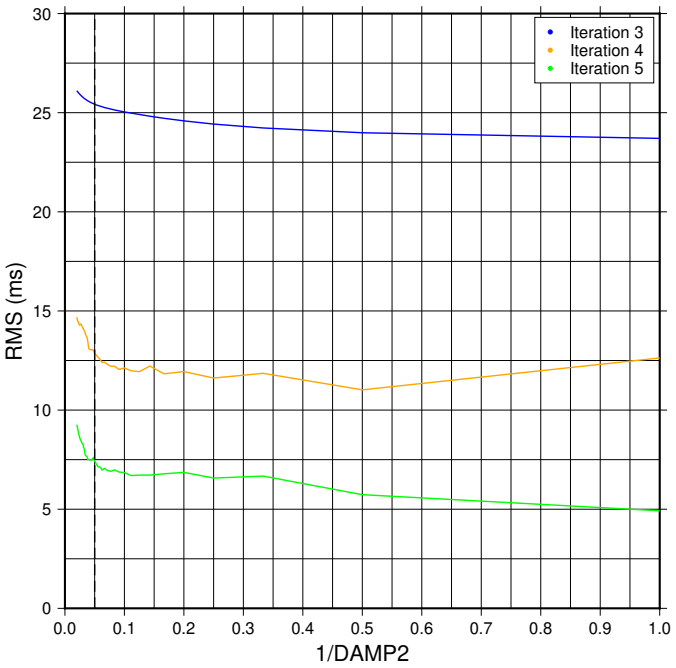

Figure E.2: L-curve optimization for the second iterative set in *HypoDD* for Loppersum.

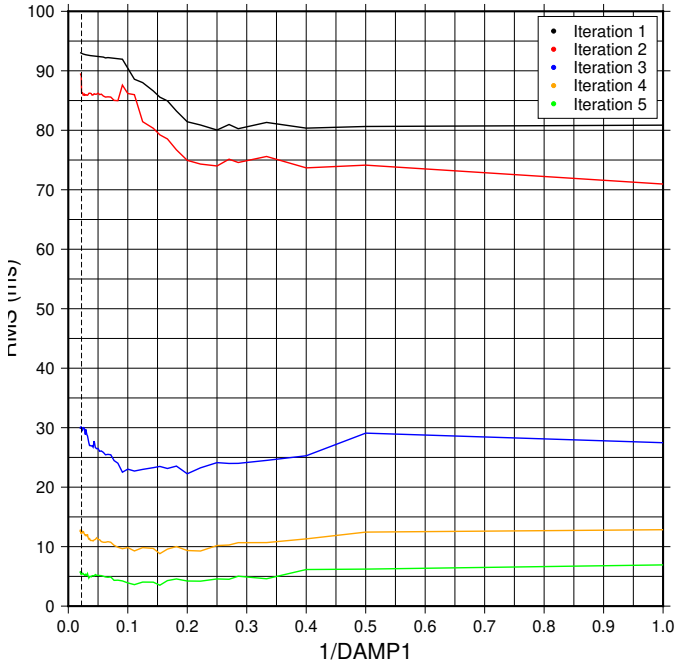

Figure E.3: L-curve optimization for the first iterative set in *HypoDD* for Groningen.

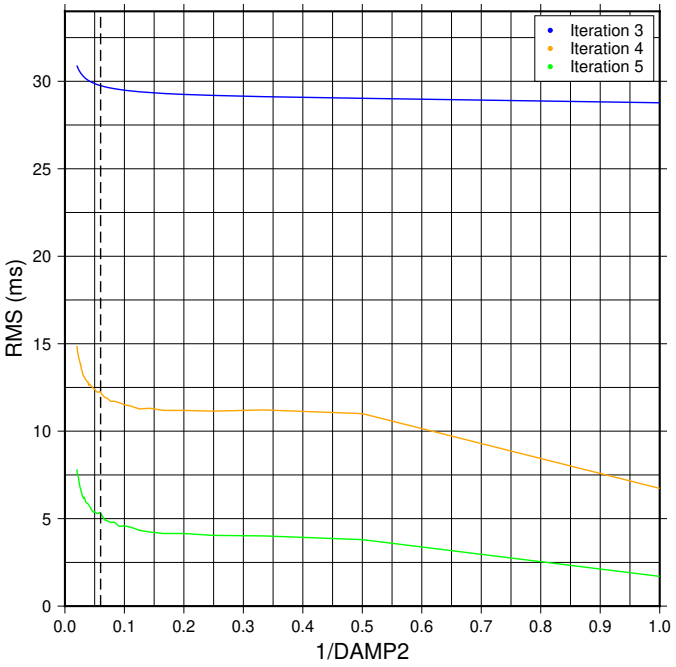

Figure E.4: L-curve optimization for the second iterative set in *HypoDD* for Groningen.

Appendix F Distance filtering and reservoir velocity effects on event depth

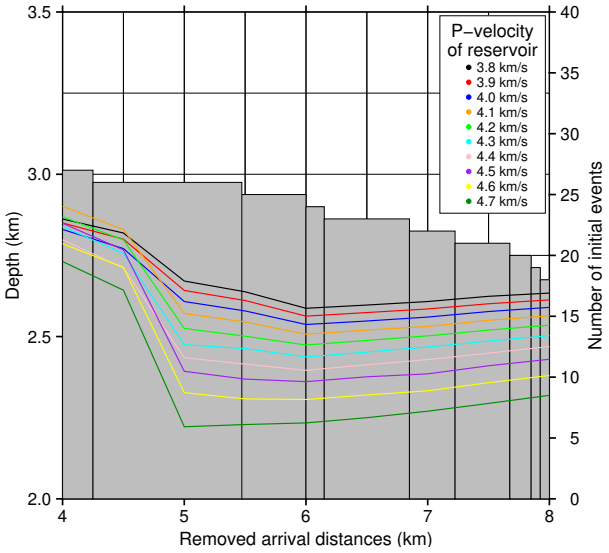

(a) The 2019/02/16 event.

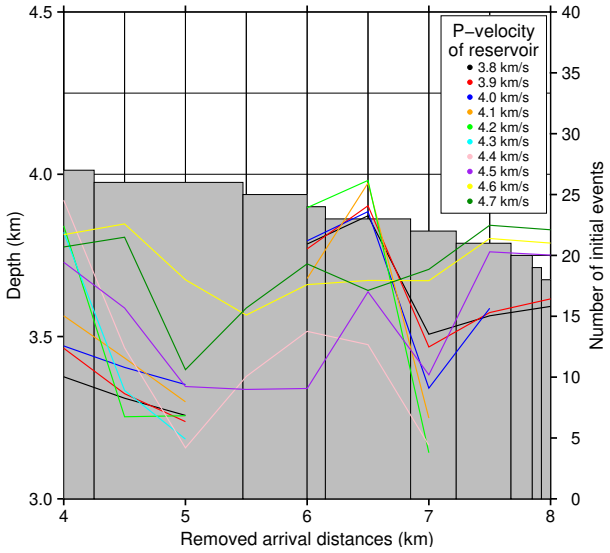

(b) The 2018/04/13 event.

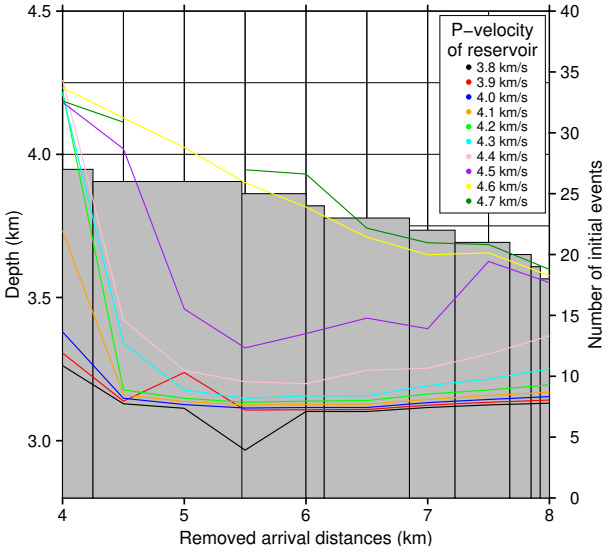

(c) The 2018/01/08 event.

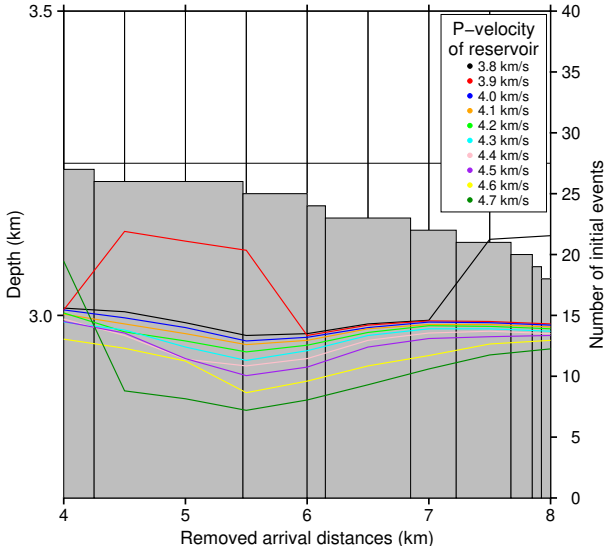

(d) The 2017/12/22 event.

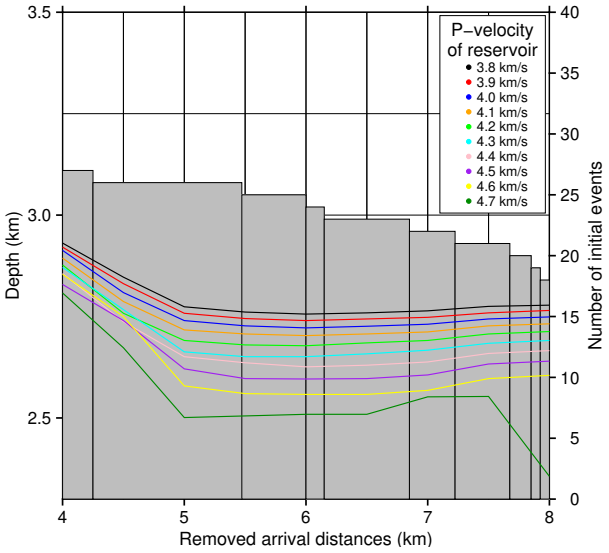

(e) The 2017/12/01 event.

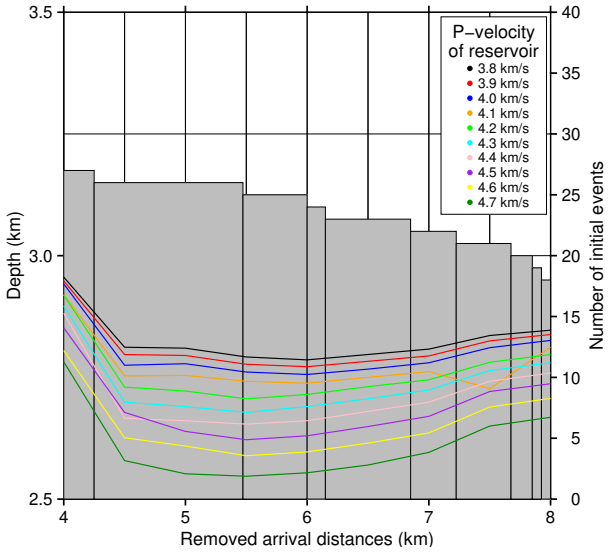

(f) The 2017/08/14 event.

(Continues on next page)

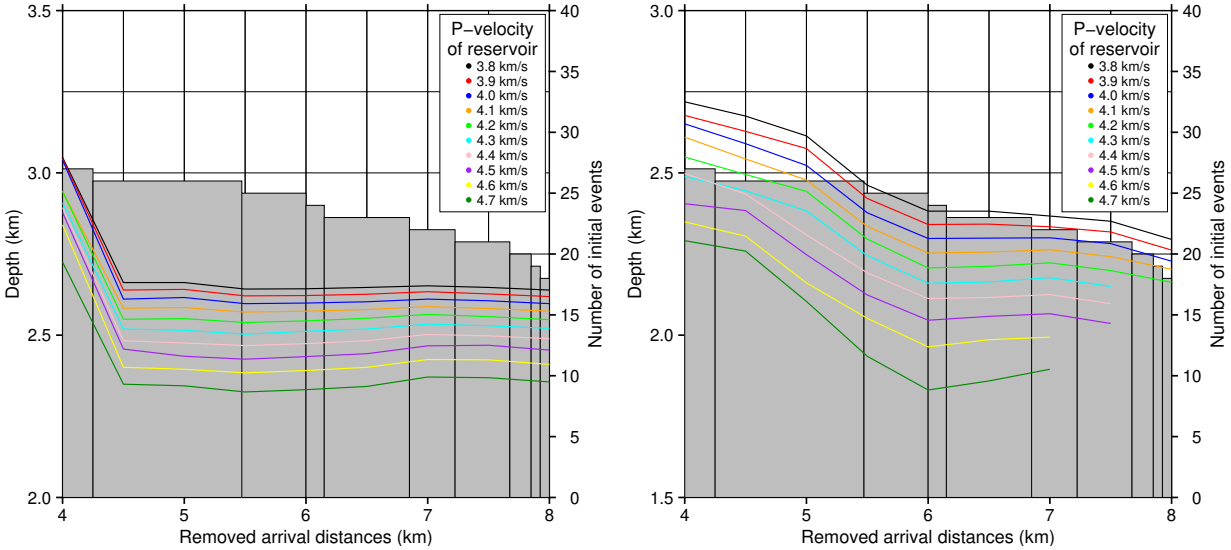

(g) The 2016/06/01 event.

(h) The 2015/11/15 event.

Figure F.1: Event relocation depths for different reservoir velocities. The gray bars correspond to the number of initial events in *HypoDD* before the inversion stage.

Appendix G Final *HypoDD* parameters

Table G.1: Final Loppersum trial area parameter settings for *HypoDD* relocation. It should be noted that cross-correlation parameter settings are left out, i.e. 0 if pre-inversion parameter and −9 if inversion parameter. The number after the parameter denotes which iterative set it belongs to.

Parameter	Value	Parameter	Value
IDAT	2	WDCT1	−9
IPHA	3	DAMP1	25
DIST	55	NITER2	3
OBSCT	8	WTCTP2	1
ISTART	2	WTCTS2	−9
ISOLV	2	WRCT2	1
NSET	2	WDCT2	1
NITER1	2	DAMP2	20
WTCTP1	1	NLAY	801
WTCTS1	−9	RATIO	1.73
WRCT1	−9	CID	0

Table G.2: Final Groningen parameter settings for *HypoDD* relocation. It should be noted that cross-correlation parameter settings are left out, i.e. 0 if pre-inversion parameter and −9 if inversion parameter. The number after the parameter denotes which iterative set it belongs to.

Parameter	Value	Parameter	Value
IDAT	2	WDCT1	−9
IPHA	3	DAMP1	45
DIST	55	NITER2	3
OBSCT	8	WTCTP2	1
ISTART	2	WTCTS2	−9
ISOLV	2	WRCT2	1
NSET	2	WDCT2	1
NITER1	2	DAMP2	17
WTCTP1	1	NLAY	801
WTCTS1	−9	RATIO	1.73
WRCT1	−9	CID	0

Appendix H Relocation of Loppersum events

Table H.1: Events that are relocated in the Loppersum area. Epicentral parameters are listed for the KNMI database together with their respective hypocentral parameters obtained with HypoDD.

			KNMI location		**HypoDD location**		
Date	**Time**	**Magnitude**	**Longitude**	**Latitude**	**Longitude**	**Latitude**	**Depth**
(yyyy-mm-dd)	(hh:mm:ss)	(M_L)	(°)	(°)	(°)	(°)	(km)
2015-06-06	23:39:15.80	1.9	6.750	53.340	6.744473	53.338436	3.170
2015-06-10	02:26:07.30	1.8	6.753	53.344	6.749529	53.347933	3.009
2015-11-15	23:01:42.84	0.9	6.743	53.357	6.744269	53.354602	2.370
2016-06-01	08:02:54.57	1.2	6.750	53.361	6.751104	53.362325	2.512
2017-02-04	02:56:52.88	0.9	6.739	53.371	6.738740	53.373250	3.189
2017-02-04	03:27:37.39	0.6	6.736	53.371	6.734223	53.375232	3.095
2017-07-10	08:44:16.59	0.7	6.741	53.332	6.740379	53.333659	3.055
2017-07-25	15:00:08.29	1.0	6.737	53.352	6.736202	53.354150	3.039
2017-08-14	03:18:59.84	1.2	6.742	53.367	6.743610	53.362276	2.694
2017-09-14	00:02:40.86	0.5	6.741	53.344	6.741071	53.343368	3.044
2017-12-01	11:33:33.34	1.7	6.736	53.360	6.739110	53.359094	2.659
2017-12-22	19:40:28.20	1.7	6.752	53.366	6.753884	53.361479	2.949
2018-01-08	14:00:52.39	3.4	6.751	53.363	6.751698	53.359534	3.173
2018-01-09	15:46:49.60	0.7	6.752	53.355	6.752488	53.357581	3.008
2018-02-08	15:25:30.53	2.0	6.751	53.335	6.750652	53.336922	3.161
2018-04-04	03:35:41.39	0.9	6.750	53.334	6.749995	53.336064	3.052
2018-04-13	21:31:35.36	2.8	6.750	53.371	6.747082	53.367428	3.334
2019-02-16	19:22:59.58	1.4	6.743	53.360	6.744148	53.363444	2.471

Appendix I Relocation of Groningen events

Table I.1: Events that are relocated in Groningen. Epicentral parameters are listed for the KNMI database together with their respective hypocentral parameters obtained with HypoDD.

			KNMI location		HypoDD location		
Date	**Time**	**Magnitude**	**Longitude**	**Latitude**	**Longitude**	**Latitude**	**Depth**
(yyyy-mm-dd)	(hh:mm:ss)	(M_L)	(°)	(°)	(°)	(°)	(km)
2015-06-10	02:26:07.28	1.8	6.753	53.344	6.747482	53.346391	3.145
2015-07-04	04:18:02.33	0.5	6.802	53.151	6.801790	53.143518	2.732
2015-07-07	03:09:00.82	2.1	6.631	53.262	6.615165	53.262944	3.110
2015-08-18	07:06:12.55	2.0	6.754	53.185	6.753634	53.184180	2.990
2015-08-28	08:07:27.84	1.3	6.584	53.392	6.834036	53.209542	2.472
2015-09-09	20:01:51.88	1.2	6.701	53.219	6.701778	53.222660	2.948
2015-10-29	06:05:10.45	0.8	6.958	53.279	6.970845	53.283785	2.654
2015-10-29	08:08:46.16	1.1	6.966	53.284	6.973370	53.283972	2.446
2015-10-30	16:07:18.87	1.7	6.776	53.294	6.776067	53.290507	2.661
2015-10-30	18:49:01.12	2.3	6.920	53.285	6.924209	53.287459	2.845
2015-11-15	23:01:42.84	0.9	6.743	53.357	6.742374	53.354215	2.526
2015-12-02	06:40:02.72	1.6	6.831	53.240	6.829312	53.237797	2.880
2015-12-03	04:40:48.38	0.5	6.641	53.250	6.652912	53.253166	1.590
2015-12-15	00:01:50.09	1.6	6.892	53.332	6.878594	53.324117	2.065
2015-12-15	07:43:54.95	1.7	6.604	53.276	6.606239	53.281181	3.801
2016-01-11	05:31:35.52	0.6	6.813	53.185	6.816137	53.178630	2.522
2016-01-13	06:41:42.32	1.3	6.855	53.248	6.852104	53.245056	2.459
2016-01-17	11:57:33.60	1.5	6.840	53.258	6.831351	53.255880	2.849
2016-01-26	22:22:33.40	1.5	6.720	53.203	6.717766	53.200761	2.866
2016-02-19	21:48:37.68	1.3	6.617	53.260	6.609042	53.261353	3.399
2016-02-20	03:44:58.95	0.7	6.627	53.355	6.618489	53.357707	2.435
2016-03-04	13:00:29.39	0.9	6.685	53.372	6.680403	53.374516	2.567
2016-03-07	10:16:53.05	1.2	6.826	53.268	6.826634	53.266333	2.697
2016-03-20	22:02:13.92	0.5	6.852	53.254	6.853882	53.254887	2.331
2016-03-24	08:00:35.71	0.6	6.879	53.290	6.875991	53.291109	1.663
2016-03-25	09:46:39.37	0.7	6.645	53.244	6.665488	53.252702	1.233
2016-04-02	00:47:53.42	1.1	6.657	53.249	6.652104	53.249772	2.791
2016-04-24	15:36:47.38	1.1	6.825	53.231	6.834125	53.228345	2.487
2016-05-16	20:38:41.90	1.1	6.916	53.291	6.911885	53.289604	2.710
2016-06-01	08:02:54.57	1.2	6.750	53.361	6.749198	53.362122	2.628
2016-06-02	18:43:13.04	1.5	6.924	53.249	6.918900	53.247274	2.899
2016-06-16	03:27:08.03	0.5	6.833	53.231	6.836656	53.229447	2.016
2016-06-18	23:58:25.12	1.2	6.766	53.184	6.767119	53.185657	2.673
2016-06-22	13:10:10.39	0.7	6.811	53.344	6.803451	53.344857	2.184
2016-07-18	08:58:11.53	1.7	6.709	53.378	6.711952	53.376550	2.764
2016-07-28	15:57:28.19	0.8	6.824	53.250	6.825347	53.250916	2.291
2016-08-07	20:40:22.08	1.3	6.644	53.374	6.645863	53.373067	2.698
2016-08-23	02:11:16.17	0.6	7.027	53.224	7.033316	53.219930	2.430
2016-08-23	03:53:30.37	1.0	7.036	53.223	7.032981	53.222709	2.674
2016-08-24	18:44:23.24	0.6	6.724	53.372	6.715895	53.372095	1.716
2016-09-09	12:21:23.42	0.8	6.811	53.337	6.810016	53.340588	1.700
2016-10-24	09:43:47.59	0.6	6.862	53.289	6.864875	53.289701	1.892
2016-11-01	00:12:28.65	1.9	6.807	53.301	6.803743	53.296370	2.765
2016-11-01	00:57:46.00	2.2	6.809	53.306	6.802883	53.297917	3.325
2016-11-05	16:58:15.87	0.8	6.940	53.266	6.943028	53.263700	2.385

(Continues on the next page)

		KNMI location			HypoDD location		
Date	**Time**	**Magnitude**	**Longitude**	**Latitude**	**Longitude**	**Latitude**	**Depth**
(yyyy-mm-dd)	(hh:mm:ss)	(M_L)	(°)	(°)	(°)	(°)	(km)
2016-11-08	11:23:17.76	1.4	6.795	53.331	6.794241	53.330119	2.370
2016-11-08	11:25:33.93	0.9	6.794	53.329	6.791722	53.330725	2.140
2016-11-20	15:20:07.76	1.0	6.744	53.299	6.735878	53.299569	2.088
2016-11-20	17:58:40.78	1.2	6.802	53.300	6.802760	53.298840	2.277
2016-12-02	08:58:21.12	0.8	6.869	53.317	6.868859	53.317529	2.268
2016-12-07	01:52:49.65	1.8	6.774	53.333	6.773154	53.327511	2.641
2016-12-15	04:44:48.83	0.6	6.807	53.343	6.802785	53.346785	2.290
2016-12-15	10:45:30.50	1.6	6.934	53.378	6.934255	53.377966	2.996
2016-12-30	03:05:53.86	1.0	6.802	53.301	6.803264	53.297770	2.584
2016-12-30	03:06:07.68	0.6	6.810	53.292	6.812899	53.295508	2.134
2017-01-14	12:47:20.00	0.6	6.840	53.214	6.840052	53.214262	1.853
2017-01-17	18:53:10.40	0.7	6.839	53.248	6.843993	53.245854	2.425
2017-01-19	22:44:47.70	0.9	6.774	53.327	6.774038	53.326331	2.321
2017-02-04	02:56:52.86	0.9	6.739	53.371	6.736153	53.373714	2.744
2017-02-04	03:11:26.71	0.8	6.657	53.368	6.650032	53.372323	2.625
2017-02-04	03:27:37.39	0.6	6.736	53.371	6.732877	53.374601	2.978
2017-02-05	15:49:33.85	1.3	6.650	53.374	6.649247	53.370793	2.784
2017-02-12	14:43:23.73	1.3	6.713	53.381	6.712267	53.376408	2.534
2017-02-14	07:45:44.23	0.9	6.672	53.378	6.670617	53.378918	2.435
2017-02-15	12:01:37.12	1.6	6.714	53.377	6.714667	53.374650	2.998
2017-02-19	13:21:25.80	1.4	6.758	53.393	6.759819	53.389982	3.067
2017-02-26	06:25:08.52	1.2	6.675	53.386	6.670407	53.378792	2.862
2017-02-26	21:39:48.72	1.4	6.778	53.328	6.777319	53.328792	2.460
2017-03-11	12:52:48.01	2.1	6.761	53.350	6.760265	53.342314	3.068
2017-04-04	10:00:44.25	1.8	6.991	53.271	7.001888	53.271139	3.899
2017-04-10	00:17:19.34	1.3	6.838	53.270	6.836685	53.269120	3.016
2017-04-10	23:37:12.92	1.1	6.989	53.269	6.999893	53.268754	4.389
2017-04-13	10:33:55.41	1.4	6.750	53.429	6.747850	53.428410	2.863
2017-04-19	17:11:08.88	0.5	6.724	53.319	6.717356	53.318746	2.995
2017-04-26	13:56:49.26	2.0	6.713	53.210	6.711635	53.208232	3.592
2017-05-03	11:15:54.14	1.5	6.727	53.312	6.722340	53.311971	3.158
2017-05-16	01:31:25.55	1.7	6.805	53.285	6.803354	53.284717	3.378
2017-05-17	07:12:33.32	0.9	6.835	53.304	6.835494	53.304545	2.376
2017-05-27	15:29:00.53	2.6	6.834	53.211	6.831555	53.205839	3.214
2017-05-30	03:44:28.67	1.4	6.750	53.433	6.750861	53.433761	3.159
2017-06-06	15:16:03.93	0.7	6.740	53.300	6.737491	53.299251	2.471
2017-06-07	00:26:10.40	1.2	6.670	53.232	6.668350	53.232926	3.018
2017-06-19	15:06:03.90	1.0	6.940	53.281	6.946590	53.281303	2.969
2017-06-29	02:13:30.87	0.7	6.724	53.316	6.718100	53.316329	2.980
2017-07-05	23:19:02.72	1.0	6.612	53.276	6.605764	53.280017	3.138
2017-07-07	02:19:36.90	0.7	6.830	53.210	6.830636	53.205994	3.067
2017-07-16	21:03:20.48	1.3	6.611	53.278	6.605593	53.279683	3.100
2017-07-21	01:22:19.97	1.1	6.659	53.381	6.658496	53.378280	2.927
2017-07-25	15:00:08.28	1.0	6.737	53.352	6.733525	53.354765	3.063
2017-08-10	10:10:29.69	0.9	6.733	53.298	6.728329	53.299023	2.939
2017-08-14	03:18:59.83	1.2	6.742	53.367	6.741516	53.361711	2.752
2017-08-17	05:38:58.84	0.8	6.748	53.423	6.751022	53.432271	3.597
2017-08-29	07:40:12.96	1.8	6.822	53.322	6.823198	53.323250	2.452
2017-09-05	22:08:27.88	1.9	6.876	53.281	6.876830	53.281478	3.140
2017-09-11	02:30:31.53	0.9	6.824	53.320	6.825728	53.323124	2.856

(Continues on the next page)

		KNMI location			HypoDD location		
Date	**Time**	**Magnitude**	**Longitude**	**Latitude**	**Longitude**	**Latitude**	**Depth**
(yyyy-mm-dd)	(hh:mm:ss)	(M_L)	(°)	(°)	(°)	(°)	(km)
2017-09-20	05:28:34.53	1.6	6.834	53.298	6.832885	53.298832	2.468
2017-09-23	19:36:42.00	0.9	6.912	53.244	6.916282	53.241536	2.945
2017-09-24	18:49:22.36	0.9	6.651	53.255	6.653000	53.255135	2.810
2017-09-30	17:15:54.48	1.1	6.727	53.241	6.728795	53.242224	3.098
2017-10-15	13:58:31.76	1.0	6.661	53.379	6.658041	53.379232	2.727
2017-10-16	22:59:24.68	0.5	6.623	53.268	6.619924	53.269714	3.195
2017-10-29	22:55:28.68	1.2	6.923	53.381	6.922190	53.380790	3.051
2017-11-03	00:12:01.62	0.8	6.821	53.177	6.823250	53.177930	2.225
2017-11-04	01:02:29.00	0.6	6.873	53.328	6.878377	53.332894	3.033
2017-11-16	18:37:58.60	0.7	6.937	53.269	6.943875	53.267985	2.977
2017-11-22	21:23:58.12	1.5	6.807	53.285	6.805086	53.284245	3.430
2017-12-01	11:33:33.33	1.7	6.736	53.360	6.737111	53.358826	2.739
2017-12-01	21:05:41.68	1.3	6.757	53.357	6.755123	53.359888	2.866
2017-12-06	23:28:59.70	1.8	6.784	53.386	6.786318	53.383138	2.938
2017-12-22	19:40:28.20	1.7	6.752	53.366	6.752061	53.360921	3.029
2017-12-24	17:49:50.64	0.7	6.833	53.305	6.835332	53.306091	2.655
2017-12-25	12:52:27.03	0.7	6.883	53.287	6.879385	53.287630	2.690
2017-12-28	14:00:30.60	1.3	6.882	53.287	6.886184	53.288005	3.028
2017-12-29	23:15:48.80	1.4	6.756	53.357	6.755681	53.361104	3.451
2018-01-01	14:46:51.09	0.8	6.884	53.287	6.885486	53.288517	2.948
2018-01-08	14:00:52.40	3.4	6.751	53.363	6.750399	53.359745	4.579
2018-01-09	15:46:49.58	0.7	6.752	53.355	6.750421	53.357483	3.043
2018-02-08	15:25:30.51	2.0	6.751	53.335	6.748347	53.336788	2.996
2018-02-10	09:58:39.78	1.7	6.710	53.228	6.708080	53.226758	3.262
2018-02-11	16:54:57.00	2.2	6.780	53.293	6.777326	53.293095	4.000
2018-02-17	08:17:30.55	1.0	6.747	53.427	6.748402	53.429281	2.580
2018-03-01	13:03:36.89	1.3	6.775	53.287	6.774934	53.286401	2.379
2018-03-10	04:13:05.74	1.3	6.861	53.314	6.862082	53.316105	2.196
2018-03-25	11:09:48.76	1.6	6.778	53.288	6.774917	53.287769	2.758
2018-03-31	06:44:03.90	1.2	6.676	53.231	6.669028	53.231669	2.197
2018-04-04	03:35:41.38	0.9	6.750	53.334	6.747562	53.336251	3.043
2018-04-13	21:31:35.36	2.8	6.750	53.371	6.745012	53.367000	4.183
2018-04-16	00:57:11.98	0.6	6.708	53.205	6.708897	53.204549	3.103
2018-05-06	16:39:06.79	1.6	6.778	53.286	6.775329	53.285522	3.980
2018-05-16	16:54:21.21	0.7	6.933	53.276	6.943193	53.278170	2.894
2018-05-21	23:27:49.24	1.6	6.795	53.374	6.797097	53.379004	2.972
2018-06-14	23:58:21.18	0.7	6.877	53.288	6.879459	53.288114	3.009
2018-06-27	14:32:52.63	1.6	6.709	53.204	6.710298	53.205725	3.623
2018-07-13	08:05:05.06	1.1	6.803	53.151	6.808103	53.145260	2.514
2018-07-19	21:45:35.18	0.5	6.713	53.207	6.712405	53.204569	3.159
2018-08-06	16:15:23.29	0.9	6.712	53.208	6.713397	53.205351	2.324
2018-08-08	02:55:29.62	1.9	6.875	53.322	6.875173	53.324715	2.464
2018-08-09	08:01:55.41	1.8	6.877	53.324	6.879063	53.327030	2.884
2018-08-13	13:48:37.10	0.7	6.838	53.207	6.841004	53.203866	3.017
2018-09-17	17:29:25.48	0.6	6.713	53.381	6.712129	53.387887	3.129
2018-09-18	02:22:59.94	0.7	6.566	53.297	6.557798	53.300073	1.950
2018-09-26	15:49:55.50	0.8	6.824	53.236	6.824238	53.232267	2.966
2018-10-16	10:31:37.68	1.1	6.858	53.252	6.854679	53.251306	3.129
2018-10-20	04:53:25.89	0.8	6.875	53.323	6.880042	53.326457	3.049
2018-10-23	14:10:53.90	0.8	6.834	53.298	6.837809	53.296981	2.995

(Continues on the next page)

		KNMI location			HypoDD location		
Date	**Time**	**Magnitude**	**Longitude**	**Latitude**	**Longitude**	**Latitude**	**Depth**
(yyyy-mm-dd)	(hh:mm:ss)	(M_L)	(°)	(°)	(°)	(°)	(km)
2018-11-09	15:41:12.38	1.6	6.680	53.367	6.674415	53.369902	2.542
2018-11-16	01:40:27.47	0.8	6.857	53.250	6.853796	53.245321	2.824
2018-11-25	19:37:37.24	1.6	6.716	53.385	6.712907	53.388033	2.842
2018-11-29	02:54:18.72	0.9	6.623	53.358	6.615088	53.361019	2.655
2018-12-11	20:50:10.86	0.6	6.617	53.277	6.613108	53.278573	2.524
2018-12-19	18:55:17.48	1.0	6.568	53.296	6.557393	53.297319	2.717
2018-12-22	04:54:11.10	1.2	6.776	53.285	6.774090	53.285087	2.963
2018-12-23	23:16:03.60	1.3	6.730	53.239	6.731566	53.239864	3.148
2019-02-01	20:41:02.56	1.0	6.727	53.242	6.726336	53.242240	3.741
2019-02-09	20:54:13.68	0.9	6.754	53.380	6.755196	53.386300	3.131
2019-02-16	19:22:59.58	1.4	6.743	53.360	6.742796	53.363139	2.571
2019-02-28	23:16:07.92	1.6	6.628	53.357	6.617598	53.358105	2.730
2019-03-29	13:37:20.80	1.5	6.654	53.369	6.647060	53.371619	2.776
2019-03-30	01:51:36.39	0.5	6.876	53.322	6.880686	53.325761	3.039